SPRING 2019
electronics-cooling.com

electronics COOLING

FEATURED IN THIS EDITION

14 MANAGING COOLING FAN NOISE IN PRODUCT DESIGN

18 USING ELECTRICAL CAPACITANCE TO EVALUATE THE THERMAL MECHANICAL STABILITY OF THERMAL INTERFACE MATERIALS

24 SPECIAL CHALLENGES IN 3D SIMULATIONS OF GRAPHITE HEAT SPREADERS

6 *CALCULATION CORNER*
PROPERTIES OF HUMID AIR

10 *THERMAL FACTS & FAIRY TALES*
WHATEVER HAPPENED TO THE PREDICTED DATA CENTER ENERGY CONSUMPTION APOCALYPSE?

© Copyright 2019 Electronics Cooling

Your partner for
thermal solutions

www.alphanovatech.com

Alpha's Extensive Products and Services

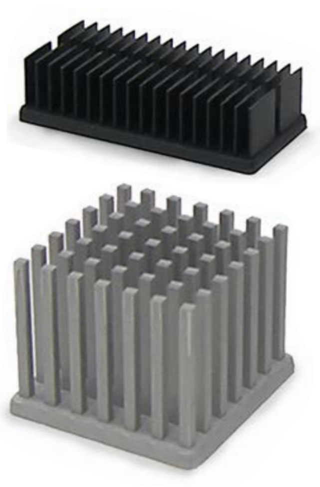

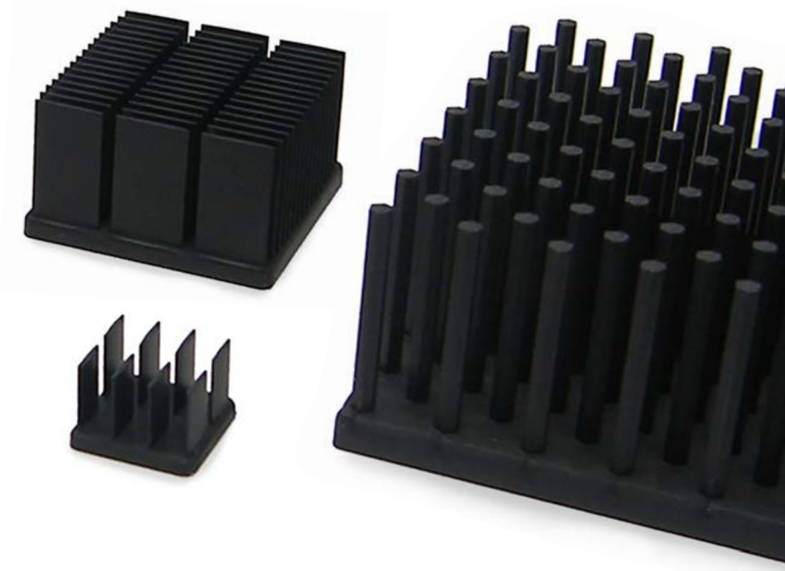

Tabbed Push Pin

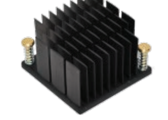
Push Pin

Shoulder Screw

QuickSet

DC-DC Converter

Optical Transceiver

CPU

LED

Push Pin

Shoulder Screw

Spring

Z-Clip

QSZ Clip

Adhesive Tape

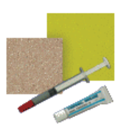
Thermal Interface

Fan

Same Day Shipping

Over 10,000 items with same day shipping.
Heatsinks, attachment hardware and accessories.

Various Attachment Options

Quickset & QSZ anchor pins require Min. PCB area.

Online Custom Design

Custom heatsinks can be designed online.
No MOQ or tooling fees. Lead time is 1-2 weeks.

Copper Embedded Heatsinks

Replacement of heat pipe/vapor chamber.

ALPHA Co., Ltd.
Head Office
www.micforg.co.jp

256-1 Ueda, Numazu City, Japan 410-0316
Tel: +81-55-966-0789 Fax: +81-55-966-9192
Email: alpha@micforg.co.jp

ALPHA NOVATECH, INC.
USA Subsidiary
www.alphanovatech.com

473 Sapena Ct. #12, Santa Clara, CA 95054 USA
Tel:+1-408-567-8082 Fax: +1-408-567-8053
Email: sales@alphanovatech.com

CONTENTS

electronics COOLING
www.electronics-cooling.com

2 EDITORIAL
Murray Slovick

4 COOLING EVENTS
News of Upcoming 2019 Thermal Management Events

6 CALCULATION CORNER
Properties of Humid Air
Ross Wilcoxon

10 THERMAL FACTS & FAIRY TALES
Whatever Happened to the Predicted Data Center Energy Consumption Apocalypse?
Bruce Guenin

14 MANAGING COOLING FAN NOISE IN PRODUCT DESIGN
David A. Nelson

18 USING ELECTRICAL CAPACITANCE TO EVALUATE THE THERMAL MECHANICAL STABILITY OF THERMAL INTERFACE MATERIALS
Lauren Boston and Andrew Yu, Timothy Chainer and Edward Yarmchuk, Michael Gaynes

24 SPECIAL CHALLENGES IN 3D SIMULATIONS OF GRAPHITE HEAT SPREADERS
Rick Beyerle

28 INDEX OF ADVERTISERS

PUBLISHED BY
ITEM Media
1000 Germantown Pike, F-2
Plymouth Meeting, PA 19462 USA
Phone: +1 484-688-0300; Fax:+1 484-688-0303
info@electronics-cooling.com
electronics-cooling.com

CHIEF EXECUTIVE OFFICER
Graham Kilshaw | graham@item.media

DIRECTOR OF MARKETING OPERATIONS
Geoffrey Forman | geoff@item.media

EDITOR IN CHIEF
Murray Slovick | murray@electronics-cooling.com

CREATIVE MANAGER
Chris Bower | chris@item.media

DIRECTOR OF BUSINESS DEVELOPMENT
Ian Quinn | ian@item.media

DIRECTOR OF BUSINESS DEVELOPMENT
Janet Ward | jan@item.media

PRODUCTION COORDINATOR
Jessica Stewart | jessica@item.media

LEAD GRAPHIC DESIGNER
Kristen Tully | kristen@item.media

PRODUCTION DESIGNER
Noah Sneddon | noah@Item.media

SENIOR COPYWRITER
Britt Schwartz | britt@item.media

ADMINISTRATIVE MANAGER
Eileen Ambler | eileen@item.media

ACCOUNTING ASSISTANT
Susan Kavetski | susan@item.media

ASSOCIATE TECHNICAL EDITORS
Bruce Guenin, Ph.D.
Consultant
San Diego, CA
sdengr-bguenin@usa.net

Ross Wilcoxon, Ph.D.
Principal Mechanical Engineer
Collins Aerospace
ross.wilcoxon@collins.com

Victor Chiriac, Ph.D, ASME Fellow
Principal Architect
Huawei R&D USA
vchiria.adrian.chiriac@huawei.com

►SUBSCRIPTIONS ARE FREE
Subscribe online at
www.electronics-cooling.com

For subscription changes email
info@electronics-cooling.com

Reprints are available on a custom basis at reasonable prices in quantities of 500 or more. Please call +1 484-688-0300.

All rights reserved. No part of this publication may be reproduced or transmitted in any form or by any means, electronic, mechanical, photocopying, recording or otherwise, or stored in a retrieval system of any nature, without the prior written permission of the publishers (except in accordance with the Copyright Designs and Patents Act 1988).

The opinions expressed in the articles, letters and other contributions included in this publication are those of the authors and the publication of such articles, letters or other contributions does not necessarily imply that such opinions are those of the publisher. In addition, the publishers cannot accept any responsibility for any legal or other consequences which may arise directly or indirectly as a result of the use or adaptation of any of the material or information in this publication.

ElectronicsCooling is a trademark of Mentor Graphics Corporation and its use is licensed to ITEM. ITEM is solely responsible for all content published, linked to, or otherwise presented in conjunction with the ElectronicsCooling trademark.

EDITORIAL

Murray Slovick
Editor in Chief

Nice to Meet You,

It is with great excitement and pride that I introduce myself as the newest member of the *Electronics Cooling* team. While my title reads "editor in chief", in actuality much of my work will be devoted to EC's online and multimedia components and I will leave the heavy lifting for the print product—finding authors and compelling high caliber articles for these pages-- to the experts on the editorial board of this publication.

It is an exciting time for me to be joining the *Electronics Cooling* community. Explosive growth in the use of electronic equipment has brought with it greater need for innovative thermal solutions and the fact that engineers have been rising to the challenge is demonstrated by steady industry gains. According to a BCC Research Report issued in February, the global market for thermal management technologies is expected to grow from $12.4 billion in 2018 to $16.3 billion by 2023 at a compound annual growth rate (CAGR) of 5.6%. In particular, the market research firm expects the thermal management hardware technologies market to expand from $9.8 billion in 2018 to $12.9 billion by 2023 at a CAGR of 5.5% for the period. Similarly, BCC's crystal ball sees the software, interface materials, and substrates market for thermal management technologies expanding from $2.6 billion in 2018 to $3.5 billion by 2023 at a CAGR of 6.1%. So things are healthy indeed.

As I enter into this "marriage" with *ITEM Media* I am taking a traditional approach. You may have heard people say you need "something old, something new, something borrowed and something blue" for your wedding day. It derives from the Old English rhyme, "Something Olde, Something New, Something Borrowed, Something Blue, A Sixpence in your Shoe"—which names the four good-luck objects (plus a sixpence for prosperity) a bride should include somewhere in her wedding outfit.

In many ways I feel I am carrying the good luck objects with me. Let's take it from the top. Something old—or since I'm already recoiling at the word, shall we say "seasoned". I come to *Electronics Cooling* with more than 20 years of experience as chief editor of award-winning publications in electro-technology. I previously was Editorial Director at Hearst Business Media with responsibility for the online and print content of Electronic Products, among other properties in the U.S. and China. I also spent a decade as editor-in-chief of the IEEE flagship publication Spectrum.

Something new. With advances in nanoelectronics and the emergence of new application areas such as three-dimensional chip stack architectures and flexible electronics, now more than ever there is need and opportunity for novel materials, techniques and technologies to help address some of these pressing thermal management challenges.

Among other new developments are thermal issues related to GaN ad SiC wide bandgap semiconductors emerging as a viable alternative to silicon, given their higher electron mobility characteristics that allow devices to be made smaller for a given on-resistance and breakdown voltage. The technology is gaining traction in power electronics and in inverters for electric vehicles.

Surely there will be unexpected breakthroughs. Introducing a game-changing technology or technique in thermal management is a bit like golfer hitting a hole in one. Both events happen relatively infrequently, yet everyone knows there's another one coming, but not exactly when or by whom. Looking at the new does not, of course, mean we will be neglect developments in tried and true cooling solutions such as heatsinks, fans, heat spreaders, thermal gap fillers, etc., which remain industry workhorses when it comes to help keeping temperatures within specified limits. We'll cover notable developments in these and other traditional cooling solutions without complacency because it is, to borrow Jefferson's eloquent phrase, a self-evident truth that in technology the only constant is change.

Something borrowed refers to, as I suggested earlier, my plan to lean heavily on the superb technical competence of our editorial board. It is not always easy to get top notch technical content and I think you'll agree that our board continues to do a superlative job.

And something blue. Isn't that a goal we all strive for in thermal management? Electronic systems are exothermic --they give off heat. A thermal camera's sensor can detect the amount of heat involved and software converts this brightness to a color scale. Usually red for the largest flux. Blue for the least flux. So blue, representing cooler regions, is certainly a good omen in our business.

Just a few more things. First, If you are planning to attend *Semi-Therm* this month be sure to stop by and say hello. Second, a bit further down the road, In October *Electronics Cooling* will again produce *Thermal Live*. The largest single thermal management event of the year features webinars, roundtables whitepapers, and videos. This is a free online event for electronic and mechanical engineers to learn the latest in thermal management techniques and topics. Please join us.

Finally, allow me to thank in advance the authors who contribute to *Electronics Cooling*, without whose continual flow of excellent submissions this publication would simply not be what it is.

– ***Murray***

SIEMENS
Ingenuity for life
Camera Module - 01
Simcenter Flotherm™ XT
• Discover a CAD-centric thermal simulation approach
• Compress the electronics cooling design process by bridging EDA & MCAD design flows
• Accurately model complex shaped geometry with robust automated meshing
Transient Simulation (Warm-up case)
Temperature (°C)
Time (s)
Cabin Air Temperature
Main Soc (Max)
Windscreen Temperature (Ave)
www.mentor.com/mechanical

COOLING EVENTS

News of Upcoming 2019 Thermal Management Events

APEC 2019

Anaheim Convention Center, Anaheim, CA, USA

APEC focuses on the practical and applied aspects of the power electronics business. This is not just a designer's conference; APEC has something of interest for anyone involved in power electronics:

- Equipment OEMs that use power supplies and dc-dc converters in their equipment
- Designers of power supplies, dc-dc converters, motor drives, uninterruptible power supplies, inverters and any other power electronic circuits, equipment and systems
- Manufacturers and suppliers of components and assemblies used in power electronics
- Manufacturing, quality and test engineers involved with power electronics equipment
- Marketing, sales and anyone involved in the business of power electronics
- Compliance engineers testing and qualifying power electronics equipment or equipment that uses power electronics

Desc. source: electronics-cooling.com
► www.apec-conf.org/about

SEMI – THERM 35

DoubleTree by Hilton, San Jose, CA, USA

Featuring Short Courses, Technical Presentations, Vendor Workshops, and much more, SEMI-THERM 35 is the place for anyone interested in networking, thermal design, and management and characterization of electronic systems and components. *Register Now!*

Desc. source: electronics-cooling.com
► www.electronics-cooling.com

ITHERM STUDENT POSTER AND NETWORKING SESSION

The Cosmopolitan of Las Vegas, Las Vegas, NV, USA

The Student Poster and Networking Session is open to all students who have an accepted technical paper, and provides opportunities for them to present their research and interact with other conference attendees from industry and academia. There will also be a networking element that allows interested students to distribute resumes and get connected to industrial representatives. Travel Grants Students who apply will be competitively selected for travel grants.

Desc. source: electronics-cooling.com
► www.electronics-cooling.com

DESIGN AUTOMATION CONFERENCE (DAC)

Las Vegas, NV, USA

The Design Automation Conference (DAC) is recognized as the premier conference for design and automation of electronic systems. DAC offers outstanding training, education, exhibits and superb networking opportunities for designers, researchers, tool developers and vendors.

Desc. source: electronics-cooling.com

► www.dac.com/

THERMAL LIVE 2019

Online Event

Thermal Live™ is the electronics and mechanical engineer's free, online resource for education and networking in thermal management. Learn the latest techniques and topics directly from thermal management thought leaders without leaving your seat. Join us for two full days of interactive webinars, product demonstrations, whitepapers, and more. Produced by Electronics Cooling® magazine.

Available now On Demand: All Thermal Live 2018 Presentations!

Desc. source: electronics-cooling.com

► www.thermal.live

IT'S SMART.
IT'S BEAUTIFUL.
AND IT'S PLASTIC.

Meet the PLQ2, our revolutionary new high-impact thermoplastic liquid cooling quick disconnect. This futuristic coupling is lightweight, chemical-resistant and easy to use. Most importantly, you'll never have to worry about drips or corrosion while on its watch.

Join the revolution, visit www.cpcworldwide/PLQ2.

©2019 Colder Products Company

CPC®
A DOVER COMPANY

Properties of Humid Air

Ross Wilcoxon
Associate Technical Editor

INTRODUCTION

Long time readers of this magazine may recall that one answer to the question of how humidity changes the thermal conductivity of air is "Nothing to worry about" [1]. Generally, the effect of humidity on air properties is small enough that it can be neglected. However, at high ambient temperatures and low pressure, humidity effects may need to be addressed in applications such as free air cooling or cooling of outdoor equipment. This article provides a method for estimating the properties of humid air, in a temperature range of 0-100˚C, and is based on a previous publication [2].

CALCULATION METHOD

Since humid air is a mixture of dry air and water vapor, it is logical that a good first step in determining its properties is to determine the properties of its constituents. These properties are dependent only on the fluid temperature and coefficients for polynomial curve fits for both fluids are summarized in *Table 1* and *Table 2*. Terms in these tables are used to calculate properties with *Equation (1):*

$$Property = \sum_{n=1}^{5} C_n * T^n \text{ where T is the absolute temperature in K} \quad (1)$$

Property	Specific Heat	Conductivity	Viscosity
Symbol	$c_{p\,a}$	k_a	μ_a
Units	kJ/kg K	W/mK	kg/m s
$C_{0,a}$	1.034090E+00	-2.276501E-03	-9.860100E-07
$C_{1,a}$	-2.848870E-04	1.259849E-04	9.080125E-08
$C_{2,a}$	7.816818E-07	-1.481524E-07	-1.176356E-10
$C_{3,a}$	-4.970786E-10	1.735506E-10	1.234970E-13
$C_{4,a}$	1.077024E-13	-1.066657E-13	-5.797130E-17
$C_{5,a}$	0	2.476630E-17	0

Table 1: Coefficients for Calculating Air Properties

Property	Specific Heat	Conductivity	Viscosity	Vapor Pressure[2]
Symbol	$c_{p,v}$	K_v	μ_v	P_{sv}
Units	kJ/kg K	W/mK	kg/m s	Pa
$C_{0,v}$	3.409770E+00	1.48E-02	-2.869369E-05	6.202781E+06
$C_{1,v}$	-1.086185E-02	-3.53E-05	4.000549E-07	-8.654308E+04
$C_{2,v}$	1.941059E-05	1.66E-07	0	4.551603E+02
$C_{3,v}$	0	-2.71E-21	0	-1.070386E+00
$C_{4,v}$	0	0.00E+00	0	9.505787E-04
$C_{5,v}$	0	0.00E+00	0	0

Table 2: Coefficients for Calculating Water Vapor Properties[1]

For example, the specific heat of air at 26.85C (300K) would be calculated as:

Cp, air = 1.034090E+00*300^0 - 2.848870E-04*300^1 +7.816818E-07*300^2 - 4.970786E-10*300^3 +1.077024E-13* 300^4 + 0*300^5 = 1.0064 kJ/kg K

Once the properties of the two constituents of humid air have been determined, they can be used to determine the properties of a mixture with a given ambient pressure, P_o and relative humidity, RH. This process requires a number of terms to be calculated: the enhancement factor (F), the compressibility factor (z), two interaction parameters (Φ_{av} and Φ_{va}) and the molar fraction of water vapor (x_v).

The interaction factor is determined using *Equation (2)*

$$F = \exp\left(\varepsilon_1 * \left(1 - \frac{P_{sv}}{P_O}\right) + \varepsilon_2 * \left(\frac{P_{sv}}{P_O} - 1\right)\right) \quad (2)$$

1. Reference [2] reported coefficients for calculating the properties of water vapor using the temperature in C. To simplify the analysis for this article, values generated with those equations were used to generate curve fits for the absolute temperature, in K.

2. The coefficients for determining saturation pressure reported in [2] seemed to have a typo that led to somewhat larger errors than reported. The coefficients shown here were generated with by generating a curve fit from the a standard steam table [3].

The constants in *Equation (2)* are calculated using the same approach as in *Equation (1)* with the coefficients shown in *Table 3.*

Property	F coeff, 1	F coeff, 2
Symbol	ε_1	$\ln(\varepsilon_2)$
C_0	-1.629131E-01	-5.987349E+01
C_1	1.805931E-03	3.436513E-01
C_2	-6.765621E-06	-7.729453E-04
C_3	8.575380E-09	6.337840E-07

Table 3: Coefficients for Calculating the Enhancement Factor

For example, for a temperature of 26.85C (300K), the two coefficients would be calculated as:

ε_1 = -1.629131E-01*300^0 + 1.805931E-03*300^1 - 6.765621E-06*300^2 + 8.575380E-09*300^3 = 0.0015 *and*

ε_2 = exp(-5.987349E+01*300^0 + 3.436513E-01*300^1 - 7.729453E-04*300^2 + 6.337840E-07*300^3) = 0.000098

At that temperature, the saturation pressure for water is calculated to be 3.56 kPa. If the atmospheric pressure is 101.35kPa, the pressure ratio P_{sv}/P_o is 0.0351 and the value of F would then be calculated as:

F = exp(0.0015*(1 - 0.0351) + 0.000098*(0.0351 - 1)) = 1.0014

Once the enhancement factor has been calculated, it can be used to determine the molar fraction of vapor for a given relative humidity using *Equation (3)*.

$$x_v = F * RH * P_{sv}/P_o \tag{3}$$

If, in the case described above, the humidity is RH=50%, the molar fraction of vapor would then be

$$x_v = 1.0014 * 0.5 * 0.0351 = 0.0176$$

The effective molar mass of the mixture, M_m, can them be determined using *Equation (4)*.

$$M_m = (1 - x_v) * M_a + x_v * M_v \tag{4}$$

Where Ma is the molar mass of air (28.97 g/mol) and Mv is the molar mass of water (18 g/mol). For the previously determined conditions then, the mixture's molar mass would be

$$M_m = (1 - 0.0176) * 28.97 + 0.0176 * 18 = 28.78 \text{ g/mol}$$

The compressibility factor, z, is a function of the temperature and saturation pressure. It can be estimated using *Equation (5)*

$$z = 1 + A * P_{sv} + B * P_{sv}^2 \tag{5}$$

The coefficients A and B are calculated using the coefficients in *Table 4*, where:

$$A = Cz_1 + Cz_2 * e^{Cz_3/T} \text{ and } B = Kz_1 + Kz_2 * e^{Kz_3/T}$$

n	Cz_n	Kz_n
1	7.0E-09	1.04E-15
2	-1.471840E-09	-3.352970E-18
3	1734.29	3645.09

Table 4: Coefficients for Calculating Compressibility Factor

For T = 300K, A = -4.700E-07, B = -6.332E-13 and z = 0.99832. Finally, the interaction parameters can be calculated using *Equations (6a)* and *(6b)*.

$$\Phi_{av} = \frac{\sqrt{2}}{4}\left(1 + \frac{M_a}{M_v}\right)^{-\frac{1}{2}} * \left[1 + \left(\frac{\mu_a}{\mu_v}\right)^{\frac{1}{2}} * \left(\frac{M_v}{M_a}\right)^{\frac{1}{4}}\right]^2 \tag{6a}$$

$$\Phi_{va} = \frac{\sqrt{2}}{4}\left(1 + \frac{M_v}{M_a}\right)^{-\frac{1}{2}} * \left[1 + \left(\frac{\mu_v}{\mu_a}\right)^{\frac{1}{2}} * \left(\frac{M_a}{M_v}\right)^{\frac{1}{4}}\right]^2 \tag{6b}$$

For a temperature of 300K, *Equations (6)* produce interaction parameters of Φ_{av} = 0.4973 and Φ_{va} = 2.4507.

Once all of these parameters have been calculated, the properties of humid air can be calculated using *Equations (7 – 10)*. These properties of the mixture of water and air include the density, ρ_m, the specific heat, $c_{p,m}$, the thermal conductivity, k_m, and the dynamic viscosity, μ_m.

$$\rho_m = \frac{1}{z} * \frac{P_o}{RT} * M_a \tag{7}$$

$$c_{p,m} = c_{pa} * (1 - x_v) * \frac{M_a}{M_m} + c_{pv} * x_v * \frac{M_v}{M_m} \tag{8}$$

$$k_m = \frac{(1 - x_v) * k_a}{(1 - x_v) + x_v * \Phi_{av}} + \frac{x_v * k_v}{x_v + (1 - x_v) * \Phi_{va}} \tag{9}$$

$$\mu_m = \frac{(1 - x_v) * \mu_a}{(1 - x_v) + x_v * \Phi_{av}} + \frac{x_v * \mu_v}{x_v + (1 - x_v) * \Phi_{va}} \tag{10}$$

For the conditions described previously, these equations calculate the properties as ρ_m = 1.171 kg/m^3, $c_{p,m}$, = 1.0162 kJ/kg K, k_m = 0.02598 W/mK, and μ_m. = 1.903E-05 kg/m s.

Figure 1 shows calculated properties for air with relative humidity ranging from 0 to 100%. Calculations are made for six combinations - three ambient temperatures are used (25, 50 and 75˚C) and two pressures (101.325 and 78.1 kPa). These correspond to sea level (s.l.) and ~2000m (2km) above sea level for a standard atmosphere.

Figure 1: Effect of Humidity on Fluid Properties

These plots show that impact of humidity on fluid properties is quite small at lower temperatures, particularly for thermal conductivity. But since hot air can hold more moisture the effects do become more pronounced at higher temperatures and lower pressures, particularly for viscosity. This is clearly illustrated in *Figure 2*, which shows the change in each property at each of the six combinations when comparing dry air (0% RH) and air with 100% RH. Again, the effects of humidity are negligible at low temperatures, but can be significant at high temperatures, particularly if the ambient pressure is low.

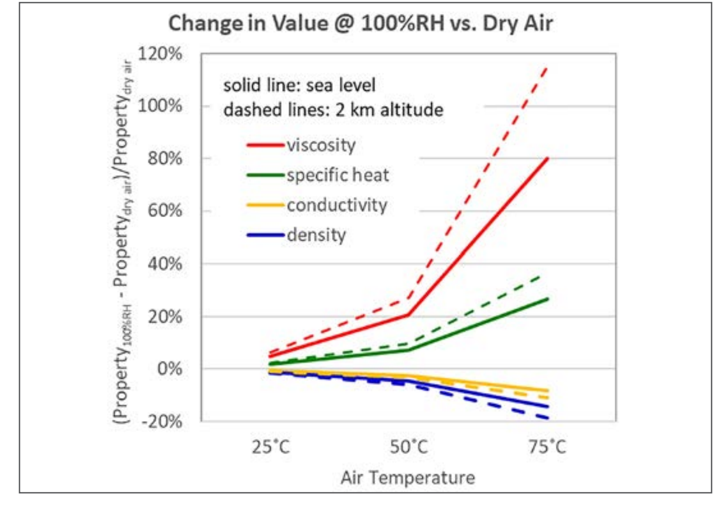

Figure 2: Comparing Properties between Dry Air and Air with 100% RH

SUMMARY

- Humidity generally has a small impact on the properties of air, but under some conditions the presence of humidity can affect properties to a sufficient degree that it needs to be accounted for.
- This article outlined a method for calculating the properties

of humid air using a number of curve fits to determine the properties of air and water vapor as well as correction factors. These curve fits were developed for a specific temperature range of 0 - 100˚C. The equations in this article should not be used outside this temperature range.

- This analysis implicitly assumes that the saturation pressure of water at ambient temperature is not higher than the ambient pressure. If this is not the case, incorrect results will be calculated.
- A spreadsheet with the procedure described in this article is available. Send an email with the word 'Humidity' in the subject line to ElectronicsCoolingWilcoxon@gmail.com to receive a link for a spreadsheet that can be downloaded for editing.

REFERENCES

1. C. Lasance, "The Thermal Conductivity of Moist Air", *Electronics Cooling Magazine, November 1, 2003*, https://www.electronics-cooling.com/2003/11/the-thermal-conductivity-of-moist-air/#
2. P. T. Tsilingiris, "Thermophysical and transport properties of humid air at temperature range between 0 and 100C", *Energy Conversion and Management*, Vol 49, pp. 1098-1110, 2008
3. 1967 ASME Steam Tables, http://www.che.ksu.edu/docs/imported/SteamTable.pdf

ACKNOWLEDGMENTS

I would like to thank *Parizad Shojaee Nasirabadi* for her help in interpreting the equations in *Ref [2]* and for recognizing the occasional typo.

With Polyonics® thermally conductive interface tapes you get maximum thermal management and excellent long-term performance under extended high temperature conditions.

- More efficient heat transfer due to low thermal resistance values of 0.37 to 0.64 °C-in²/W
- Continuous operating temperatures up to 437 °F (225 °C)
- Long term durability with 1,000-hour testing at 437 °F (225 °C)

polyonics.com/VeryCool
for more information and to request samples.

603.352.1415 | info@polyonics.com

Whatever Happened to the Predicted Data Center Energy Consumption Apocalypse?

Bruce Guenin
Associate Technical Editor

INTRODUCTION

As the title indicates, since the middle of the last decade, there have been very pessimistic projections regarding the growth of the total annual energy used by data centers in the U.S. One of them suggested that by 2030, the energy consumption in the U.S. in the IT sector would be roughly 60% of that used by its entire industrial sector. [1,2,3]

What was the origin of this dire prediction? How is it holding up in light of more recent data?

The first early warning of this risk resulted from a very comprehensive U.S. Environmental Protection Agency (EPA) energy report, released in 2007.[1] It did chronicle the very rapid increase in the annual energy use by data centers in the U.S. In fact, the reported annual rate of increase was 15% . This translates into a doubling of energy consumption in only 6 years and a tripling in 9 years. In addition to documenting energy use from 2000 to 2006, it also made predictions about the what the future would hold for us, subject to different technical assumptions. *Figure 1* provides a graph from their report.

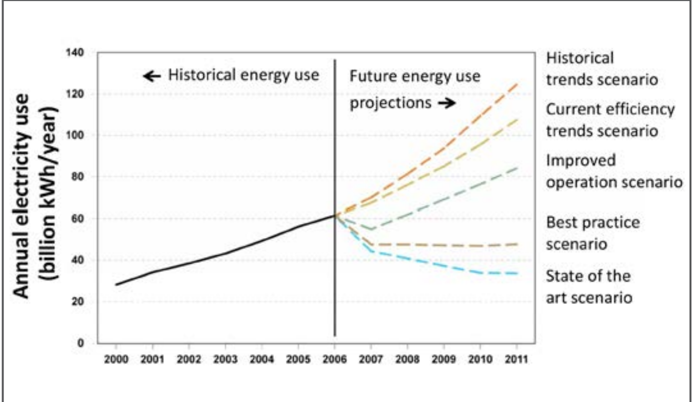

Figure 1. Comparision of Projected Electricity Use, All Scenarios, 2007 to 2011. [Fig. ES-1, Ref.2]

The predictions reflect a very nuanced analysis of what the future might hold. The trajectory of highest energy growth makes the assumption that energy consumption would continue at the very high rate manifested by their recent history. The implication is that there would be no improvement in efficiency in any aspect of running a data center. To accommodate the expected continued growth in data centers, companies would simply make more of the kinds of servers and infrastructure they had been doing in their recent past. Of course, on a moment's reflection, one sees that this would be an absurd assumption, but it was provided nonetheless, since it should represent a worst-case situation and would therefore represent an upper bound on energy consumption. Then, as the possibility of efficiency improvements in various technical areas was accounted for, the trend line became less steep and, in the most optimistic case, actually showed a decreasing trend.

Not too surprisingly, it was the worst-case scenario that was picked up by the media and also various analysts.[4] This became the trend line that was most commonly used for forecasting energy trends.

To analyze energy use since 2006, we make use of data extracted from a recent monumental study, conducted by the U.S. Department of Energy, that looked at power consumption while considering all aspects of data center IT configurations, equipment, and cooling practices over the full range of data center sizes.[5] This report provided actual energy consumption values for data centers up to the year 2014. It also makes predictions out to 2020 for various scenarios, representing a spectrum of assumptions regarding increases in the energy efficiency both in servers themselves and in all aspects of the infrastructure. It was the first report to quantify data center energy use over the entire U.S.

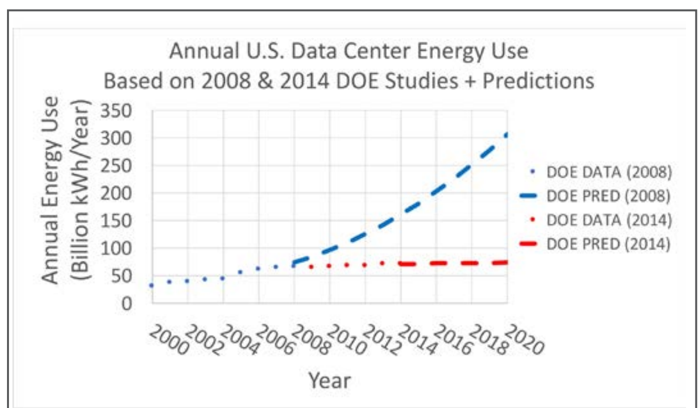

Figure 2. Comparison of Actual and Projected Energy Use in U.S. Data Centers, 2000 to 2020. [Based on data in Refs. 2, 5]

The graph in *Figure 2* plots actual energy usage data from 2000 to 2014 extracted from the report. This shows a much more benign

behavior than the worst-case projection plotted in *Figure 1*, which is represented by the dashed blue line in this graph. The projection of energy use from 2014 to 2020 is represented by the dashed red line that appears as a horizontal continuation of the recent data.

This report shows that, indeed, the many doomsayers in the media who took a worst-case scenario and institutionalized it were completely wrong. Rather than representing a steep, exponential increase in energy, the trend is linear with a slight upward slope, increasing by 1.6% per year.

It makes one wonder how so many people could have been so wrong. Fortunately, the 2014 DOE report provides an exhaustive analysis of the many factors affecting energy consumption by data centers. We'll look at those shortly.

One benefit of the expected exponential growth in energy consumption was that it created a lot of concern in many sectors of our society. Naturally enough engineers shared this concern as well.

Faced with this alarming trend, engineers began to worry not only about the power consumed by the computing and networking electronics, but also about the power used to operate the fans, air conditioners, and other cooling equipment. The term PUE (Power Usage Effectiveness), a measure of data center cooling efficiency, was defined in 2006. It is defined as:

PUE *= Total Facility Energy Consumed / Energy Powering the IT Equipment*

For example, PUE = 1 if all the energy powers the IT equipment and PUE = 2 if amount of energy devoted to cooling equals the energy for powering the IT equipment.

PUE analyses immediately began to be broadly applied to data centers. The ratings were, in general, initially closer to 2 than 1. Quantifying the problem led to broad thinking about how to reduce it. It prompted a lot of analysis and subsequent action on how to reduce energy consumption.

Figure 3, from the 2014 report, shows the past and projected growth rate of total U.S. data center energy use from 2000 until 2020, which is represented by the solid black line. There were various inflection points of note: 1) in the 2008 time frame, the energy consumption trend line bent so that the 15%/year slope was reduced to only 4%/year. This was mainly due to a smaller installed base of servers due to the economic recession and the related efficiency improvements driven by pressures to reduce energy and equipment costs. However, in the year 2010, as data center capacity began to increase again, the energy growth rate was less than 2% per year. The dotted line ascending from the actual trend line in 2010 represents the predicted growth in energy consumption if there were no efficiency improvements in IT hardware and infrastructure after 2010.

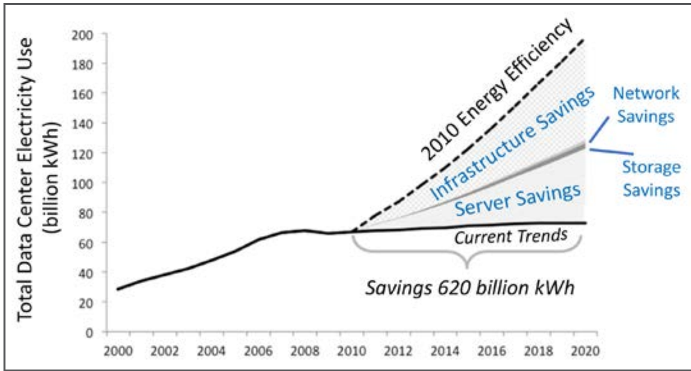

Figure 3. Data Center Electricity Consumption in Current Trends and 2010 Energy Efficiency Scenarios [Ref. 5, Fig. 24.]

This graph also quantifies the effect of improvements in energy efficiency in four major classifications of the IT infrastructure: servers, infrastructure, network, and storage. They are discussed below, in order of significance:

- Infrastructure – this deals mainly with cooling and power conversion and backup power, with cooling accounting for most of the energy usage. Readers of this publication will know of many ways in which the process of cooling IT equipment can be made more energy efficient. Better management of the incoming cool and outgoing warm air streams alone can account for significant savings. Also, introducing liquid cooling in as many sections of the heat flow path, as is practical, from the computing hardware to the outdoor environment can greatly enhance efficiency.
- Servers – energy savings are provided automatically by Moore's Law scaling, as the energy required to implement a specific computational workload decreases with time. There are also advances in server computation architectures in enabling virtualization, that facilitates the routing of computational work to a specified server so that it operates at a high utilization rate. This not only reduces the total number of servers needed, it also improves the power efficiency. Those remaining servers operating at a low utilization rate are designed to significantly reduce their power consumption during those periods.
- Network – there are two factors responsible for reducing the energy required to transmit a given quantity of data over IT networks: 1) Increasing bandwidth. For example, in a given generation of silicon, increasing bandwidth from 10 to 40 Gb/s only increases the power by a factor of 1.7. 2) At a given bandwidth, for example 40Gb/s, Moore's Law scaling provides roughly a 13% power reduction per year, that, over 6 years, reduces the power by 50%.
- Storage – The biggest contributor to the reduction in energy consumption by storage devices is the fact that the capacity in an individual device has been increasing at a rapid rate. This allows a smaller number of drives to meet a specific storage requirement than were required in the past.

There is another dynamic that was operative in reducing the

energy use by data centers since 2010, namely the trend in which the larger data centers continue to account for a higher share of the total number of the servers in the U.S. The following Table divides the data centers in the U.S. into 6 categories, ranked by the floor area in each center.[6]

Table -- Data Center PUE Values				
Data Center Size Category	Typical Size		PUE Values	
			2014 (Actual)	2020 (Per Current Trends)
	(m^2)	(ft^2)		
Internal Server Closet	< 9.3	< 100	2.0	2.0
Internal Server Room	9.3-92.8	100-999	2.5	2.35
Localized Data Center	46.5-186	500-1,999	2.0	1.88
Mid-Tier Data Center	18.6-1,858	2,000-19,999	1.9	1.79
High-end Data Center	>1,858	>20,000	1.7	1.6
Hyperscale Data Center	Up to over 37,161	Up to over 400,000	1.2	1.13

They range from the classification of an "Internal Server Closet" whose size is under 9.3 m^2 to a Hyperscale Data Center, whose size ranges from 1,900 to over 37,000 m^2. The Internal Server Closet would be found at a small company to satisfy its internal IT needs. The hyperscale data centers would include the cloud computing and internet giants such as Google, Facebook, Amazon, and Microsoft.

The PUE values tend to be higher the smaller the data center. It is noteworthy that only the hyperscale data centers have PUEs near 1. The high-end data centers have values has a value of 1.7. All of the smaller ones have values in the range, 1.9 to 2.5. Furthermore, one expects only a small improvement in their PUEs by 2020.

The hyperscale data centers have been designed from the ground up to have maximum cooling and power conversion efficiency and often incorporate selective liquid cooling.

The smaller data centers lack the economies of scale of their hyperscale cousins. They typically are entirely air cooled and often have suboptimum air flow conditions where there is poor separation between hot and cold air streams, leading to hot spots. Lacking the resources to better manage air flow, the common practice is to deal with the hotspots by overcooling the datacenter. With the emphasis on avoiding downtime rather than minimizing the power consumption devoted to cooling, these data centers tend to have higher PUEs.

This macrotrend involving the migration of data center energy consumption from the smaller data centers to the large ones is captured by *Figure 4.* Of course, from an energy utilization perspective, this is a positive trend since the largest data centers get considerably more computing work per watt than do the smaller ones.

In spite of this trend, the report estimates that in 2020, 40% of the total energy will be consumed by data centers at the mid-tier size and smaller, with their lackluster PUEs of 2. Clearly, improving the energy efficiency of these small data centers would represent an opportunity for the thermal management community. It should be mentioned that in the future, there will be an increasing number of small-size data centers that will migrate to the cloud. As the preceding analysis indicates, if implemented at a cloud computing provider, their computational workload should be executed in a more energy efficient way than was possible in the original data center.

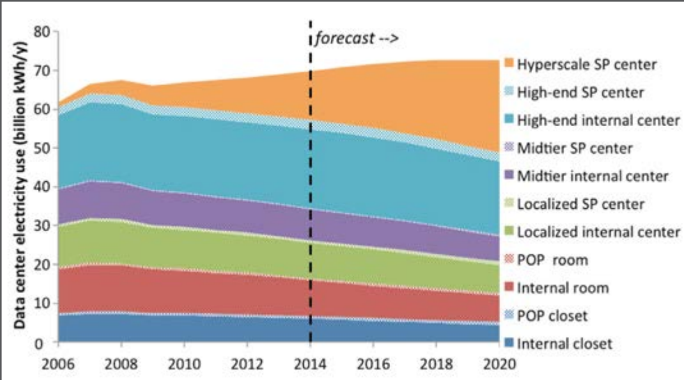

Figure 4. Data Center Annual Electricity Consumption Differentiated by Size Category [Ref. 5, Fig. 22]

CONCLUSIONS

This analysis provides some comfort in that we can expect that, in the near future, total energy consumption by U.S. data centers should be very manageable. However, we can expect that as the data center sector in the U.S. scales up to accommodate the computational and data management requirements of the Internet of Things, we will once again be challenged by the sheer scale of this enterprise and its immense energy needs.

REFERENCES

1. Report by the U.S. Energy Information, Report#: DOE/EIA-0383(2008), Release date full report: June 2008; Next release date full report: February 2009.
2. Report to Congress on Server and Data Center Energy Efficiency Public Law 109-431 U.S. Environmental Protection Agency ENERGY STAR Program, August 2, 2007. http://www.energystar.gov/ia/partners/prod_development/downloads/EPA_Datacenter_Report_Congress_Final1.pdf
3. Madhusudan Iyengar and Roger Schmidt, "Energy Consumption of Information Technology Data Centers," ElectronicsCooling, Vol. 16, No. 4, December, 2010.
4. Patrick Thibodeau, "Data centers are the new polluters," Computerworld, Aug 26, 2014 https://www.computerworld.com/article/2598562/data-center/data-centers-are-the-new-polluters.html
5. Arman Shehabi, et al. "United States Data Center Energy Usage Report," Lawrence Berkeley National Laboratory Document Number LBNL-1005775. http://eta-publications.lbl.gov/sites/default/files/lbnl-1005775_v2.pdf]
6. Bruce Guenin, "Data Center Power Trends – Where Do We Go from Here?," Editorial, ElectronicsCooling, June, 2018.

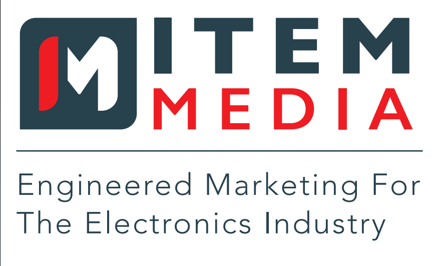

Understand your customers' digital footprints to better understand their journey.

- Lead Qualification
- Lead Generation
- Audience Development
- Online Events
- Content Creation
- Technology Implementation
- Big Data Translation
- *...and MORE!*

Start your journey today!

please visit

item.media

Additional ITEM Media Brands: Interference Technology | Electronics Cooling | Environmental Test & Design

Managing Cooling Fan Noise In Product Design

David A. Nelson
Nelson Acoustics

ABSTRACT

Cooling fan noise is a system property determined as much by thermal and mechanical design and fan selection as by a fan's acoustical design. While even the quietest fan can be used in a noisy manner, a significant fraction of unpleasant surprises can be avoided.

KEYWORDS

Cooling fan, noise emission, acoustics, sound power

NOMENCLATURE

C	Numerical constant
D	Impeller diameter [m]
c_P	Specific heat [J/(kg °K)]
A_D	Reference duct area (1 sq. meter)
I	Installation Effects [dBA]
K_{WA}	Specific Sound Power Level [dBA]
L_{WA}	Sound Power Level [dBA]
N	Rotation speed [s^{-1}]
q_H	Heat generated [W]
P_S	Static pressure rise [Pa]
R	Backpressure coefficient
T_X, T_I	Exhaust and inlet air temperatures [°C]
$\dot{V}$	Flowrate [m^3/s]
ΔK_{WA}	Change in Specific Sound Power Level [dBA]
ξ	Bypass ratio
φ	Non-dimensional flow coefficient=$\dot{V}/(.078ND^3)$
φ_0	Optimal non-dimensional operating point
ρ	Air density [kg/m^3]

INTRODUCTION

Interest in and concern about cooling fan noise is increasing due to increasing power density, decreasing package size, and greater customer sensitivity to noise. It's not uncommon for thermal engineers to find themselves with a late prototype system that doesn't meet noise emission goals, necessitating a search for a "quiet fan". This quest is often perplexing, because fans that were quiet in a similar product or application, or appear to be quiet in a catalog, often don't deliver the hoped-for performance.

The insight needed to achieve quiet fan cooling is found at the intersection of acoustics and thermal engineering. Cooling fan noise emission is a *system* property influenced as much by the thermal design, including heat generation, conduction, and exchange, as by the "quietness" of the fan.

The bad news is that certain early design decisions can unwit-

1. The sound power emitted is analogous to watts or BTU, and is expressed as sound power level in dB referenced to 1 picowatt. Sound pressure level, like temperature, depends on location, environment, and many other factors.

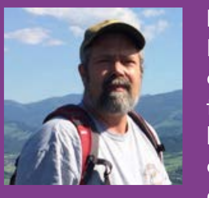

David A. Nelson | david@nelsonacoustical.com, (PO Box 879, Elgin TX, 78621 USA)
David A. Nelson is principal consultant of Nelson Acoustics, near Austin, Texas, and has been active in the world of acoustics for 40 years, including twenty-five as an acoustical consultant. He applies and teaches noise control from a unique perspective: by designing to control noise at its source before it's created and by addressing human perception (i.e., "sound quality"). David has applied these techniques to information technology equipment, consumer products and appliances, a leaf blower, medical diagnostic and surgical equipment, air conditioning and refrigeration products, spaceflight experimental hardware, and theatrical lighting. His more general noise control work encompasses a wide variety of situations in buildings, industry, and the environment. David delivers practical, customized training seminars on acoustics and noise control topics to engineers and decision-makers. He holds a BS (MIT) and MSE (UT Austin) in Acoustics, is Board Certified by the Institute of Noise Control Engineering, a Professional Engineer, an Instrument-rated Private Pilot, and an accomplished musician.

tingly "bake" noise into a system. The good news is that such outcomes can be foreseen, and a noise-conscious design process can increase the likelihood of success.

NOISE EMISSION OF COOLING FANS

Five major factors determine the noise emission of an air mover[1]. These are joined in a simple empirical equation for A-weighted sound power level L_{WA} [1,2]:

$$L_{WA} = 50 \log \dot{V} + 20 \log R + K_{WA}(\phi_0) + \Delta K_{WA}(\phi) + I + C \quad (1)$$

where C is -4 for flowrate in m^3/s and -185 if in cfm. In either case, standard atmospheric density and a reference duct area (A_D) of 1 square meter are assumed.

The first factor in *Equation 1* is a direct consequence of the thermal design, which determines the required flowrate:

$$\dot{V} = \xi \frac{q_H}{\rho c_P \left(T_X - T_I\right)} \quad (2)$$

Flowrate in turn depends upon many factors that thermal engineers regularly manage including heat rejection (q_H), bypass flow ratio (ξ), heat exchanger design (T_X – T_I), and inlet air temperature T_I.

Changes in the thermal design that alter the required airflow can influence the likely noise emission by several dB.

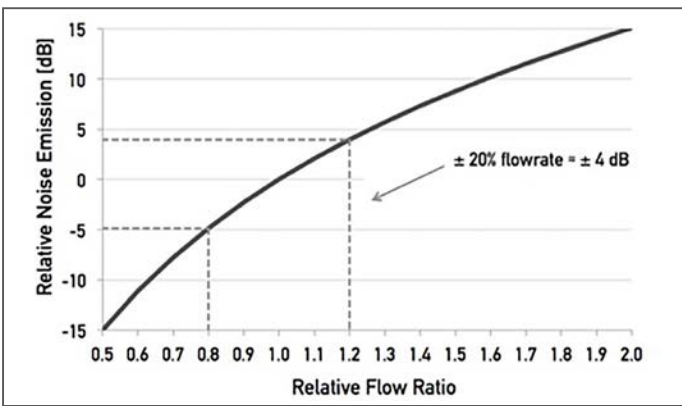

Figure 1: Relative noise emission vs. flowrate

The second factor is the non-dimensional, turbulent-flow chassis backpressure coefficient R, determined from:

$$P_S = \frac{1}{2}\rho R\left(\frac{\dot{V}}{A_D}\right)^2 \quad (3)$$

Changes in backpressure can also influence the likely noise emission (see *Figure 2* following).

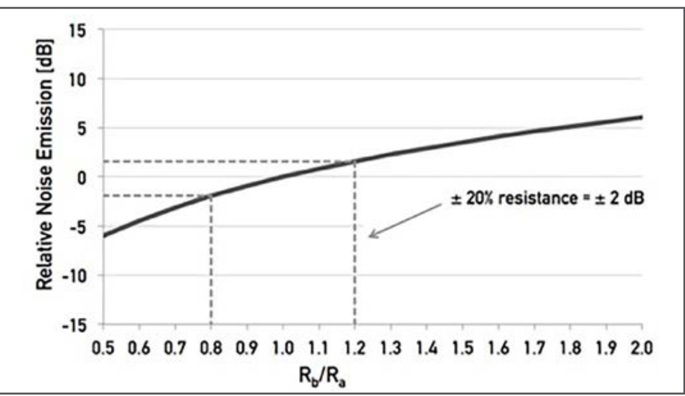

Figure 2: Relative noise emission vs. backpressure coefficient

The third factor expresses the fan's intrinsic noisiness in terms of its "specific sound power level" K_{WA}, which applies at its quietest operating point (near maximum static efficiency). Typical axial fan K_{WA} values are around 60 with "quiet" and "noisy" fans ranging 10 dBA below and above this average, respectively. Centrifugal blowers and centrifugal fans can be significantly quieter than axial fans (6 and 15 dB lower respectively on average); but may not fit well into systems designed around axial fans.

The specific sound power level K_{WA} is determined from L_{WA} at each operating point as[2,3]

$$K_{WA}(\phi) = L_{WA}(\phi) - 10\log(\dot{V}) - 20\log(P_S) \quad (4)$$

K_{WA} values depend on the units of flow and pressure used to generate them. Care should be taken that they be used consistently and not mixed in equations with other flow and pressure units.

The fourth factor addresses the fact that a fan emits additional noise when it is not well matched to the load (non-optimal operating point). *Figure 3* shows an example of a typical fan in which this factor can cost 5 dB or more.

The fifth factor combines several less-predictable factors brought about by installing the fan into a real system. These typically include inlet flow distortions such as uneven flow distribution and turbulence ingestion, as well as partial shielding of the fan by the chassis. Flow distortions change the interaction between streamlines and fan blades that can increase the effective K_{WA} and reduce flow delivery. In such a situation the fan speed has to be increased to produce the required flow, resulting in yet more noise being generated.

2. Laboratory fan test setups are assumed to have negligible installation effects. When inlet and outlet conditions are mocked up, the ΔK_{WA} encompasses installation effects.

3. A-weighting is a filtering process that emphasizes high frequency energy and seeks to imitate human perception of loudness (at low levels) or the potential for hearing damage (at high levels). Levels obtained using this weighting are expressed as dBA.

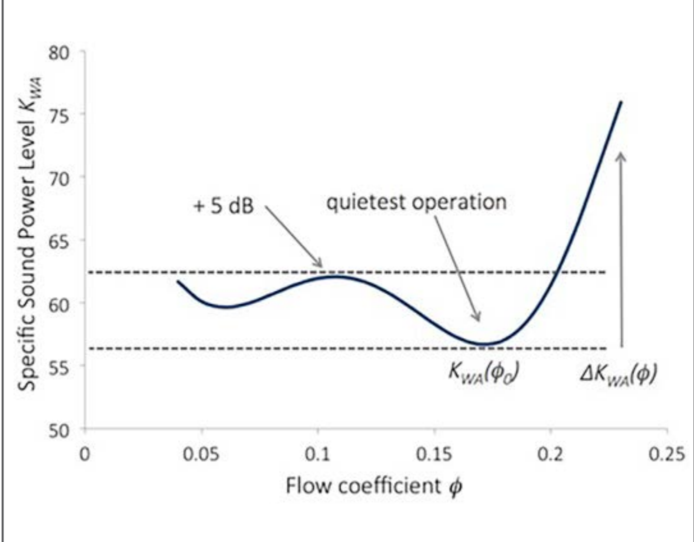

Figure 3: Typical $K_{WA}(\varphi)$ vs. operating point

Taken together these five factors can explain many otherwise surprising disappointments. The demands placed upon a fan by the thermal and mechanical designs are at least as important as the acoustical design features of the fan. Even the quietest fan could be rendered noisy if implemented poorly or operated at high speed. Conversely, a rather ordinary fan can appear to be "quiet" when it is used well in a less-demanding system.

CONSEQUENCES FOR DESIGN

Design engineers already possess the skills needed to make fan-cooled systems quieter, even without any knowledge of acoustics. Yet the constraints of typical projects often lead them to unwittingly design high noise levels into their products. These decisions usually occur very early in the design process, and it's not always possible to overcome them later by finding a "silver bullet" quiet fan. Because of the intertwining nature of thermal and mechanical design with noise, an integrated approach is necessary to achieve success.

Even apparently minor and unrelated design decisions can be important. In one example [3], a less thermally resistive TIM reduced by 15% the airflow requirement for a CPU/ASIC package. The minimum fan speed for adequate cooling decreased from 3900 to 3300 RPM, and the noise emission dropped with it by about 5 dBA.

Figure 4 shows the effective thermal resistance (blue and red lines) vs. RPM for the two TIM materials, with a target overall resistance of 0.295 °C/W. The green line shows sound pressure level (dBA, right axis) for the two RPMs and the resulting noise reduction.

In another example, design review of a large and unexpectedly loud server rack revealed that it was 19 dBA louder than necessary. Of this, only 4 dBA was due to a higher-K_{WA} fan. Poor load-matching and avoidable flow blockages accounted for another 4 dBA. The remaining 11 dBA was directly related to poor heat exchanger efficiency and excessive thermal resistance. [1]

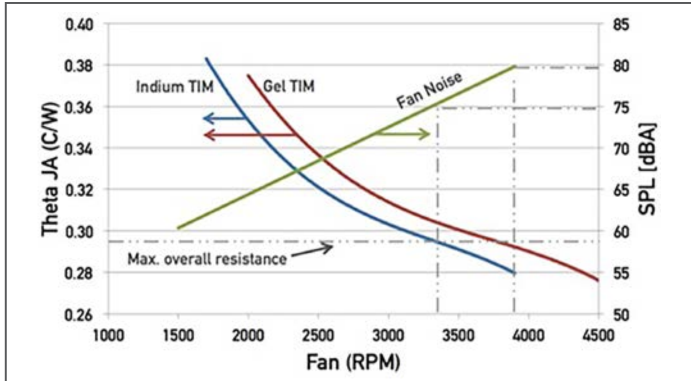

Figure 4: TIM Selection vs. Noise Emission (adapted from [3])

RATINGS

It has long been customary to rate fan noise according to its A-weighted sound pressure level, 1 meter upstream along the rotational axis, suspended in a hemi-anechoic chamber. It's a straightforward but highly unrealistic setup: the fan is subjected to no load and interacts with pristine inflow and outflow conditions.

More meaningful data can be obtained from measurements according to ISO 10302 [4] (for small fans) and ISO 13347 [5] (for larger fans). The global sound power level is measured under various realistic load conditions simultaneously with aerodynamic performance. Some fan manufacturers are beginning to include A-weighted sound power level data in their catalogs; more detailed acoustical analysis (e.g., tonality) is also possible and such data may also be available. Best of all, realistic inlet and outlet conditions can be mocked up to better simulate critical applications.

Equation 4 can be inverted to anticipate noise-related constraints. For example, we can plot the locus of pressure-flow states for candidate fans with K_{WA} of 35, 40, and 45 (dBA), that just deliver a maximum permissible 80 dBA sound power level. The system curve is laid across these loci (500 Pa @ 0.1 m3/s). The points of intersection represent the maximum flow achievable within the noise constraint for each case, approximately 0.100, 0.075, and 0.060 m3/s, respectively. This illustrates both the benefit of quiet fans and the ability to infer thermal and mechanical design goals.

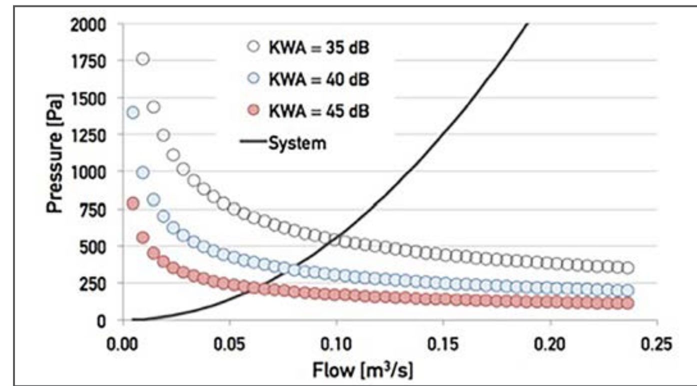

Figure 5: Pressure-flow combinations that meet 80 LWA

CHARACTERISTICS OF QUIET AXIAL FANS

Low-K_{WA} axial fans cannot be reliably identified based on how they look. Only acoustical data can answer that question. Certain visible characteristics are common in quiet fans, but may not by themselves guarantee quiet operation. Other subtle characteristics may actually be more important.

Aerodynamic blade design: Laminar airflow is quietest. Blades that change their pitch (twist) and chord (width) between hub and tip promote laminar flow by managing the relative vector velocities of the incoming airflow and advancing blade.

Tip gap: Close machining tolerances permit a tight gap between tip and shroud. Air that backflows around the tips creates noise and also requires that the fan be sped up to recover the lost airflow [6].

Curved vs. Straight blades: A curved leading edge may help reduce the relative strength of blade pass tones.

Serrated trailing edges reduce noise by disrupting the uniformity of the air leaving the trailing edge, but trailing edge noise is only one of several mechanisms of fan noise generation.

Stacked fans: are popular in systems with high backpressure. The downstream (secondary) fan ingests spiraling, turbulent discharge airflow from the primary. In co-rotating fan pairs, the secondary fan blades chase the flow and generate the same or more noise but scant additional airflow. A flow straightener (or a wide gap) may allow an identical secondary fan to perform as if it were independent. In counter-rotating pairs, the secondary fan usually looks noticeably different in order to efficiently handle the spiraling inflow. Systems that require stacked fans are potential candidates for conversion to centrifugal formats.

Fan dimensions: Fan dimensions have an indirect bearing on noise emission because they influence the compatibility with the system through the ideal operating point. Diameter, thickness, and hub ratio all play a role. All things being equal, thinner axial fans deliver less flow than thick ones, and large hubs are optimized for higher pressure than small ones.

CONCLUSION

- No fan is so quiet that it can be relied upon to save a noisy system after the fact.
- Baseline noise emission is determined by the thermal and mechanical designs as well as the space allotted for the fan and its assigned format (axial, centrifugal).
- Sound power level (L_{WA}) data obtained at representative loads is more meaningful than unloaded, on-axis sound pressure level data.
- A low-K_{WA} fan, selected to match the system operating point, and implemented with minimal installation effects, gives the best results.
- Quiet operation and low energy consumption go hand in hand.
- You can't tell if a fan is quiet by how it looks.
- Two fans that look identical need not have the same performance and noise emission.
- Just because a fan was quiet in another system doesn't mean it will be quiet in your system.
- Just because a fan was quiet in last year's system doesn't mean that it will remain quiet if heat generation increases.
- All things being otherwise equal, fan noise goes as 50 log (RPM).

REFERENCES

1. D. Nelson, Reducing noise by managing heat, Proceedings of Noise Con 2016.
2. D. Nelson, In Search of a Quiet Fan, Proceedings of 34th IEEE Semi-Therm Symposium, 2018.
3. M. Vogel, J. Galloway, D. Nelson, "Improved router & server OPEX, acoustics and leakage power through advancements in ASIC/CPU design", Proceedings of 32nd IEEE Semi-Therm Symposium.
4. ISO 10302 – Acoustics - Measurement of airborne noise emitted and structure-borne vibration induced by small air- moving devices – Part 1: airborne noise measurement.
5. ISO 13347 – Industrial Fans – Determination of fan sound power levels under standardized laboratory conditions
6. W. Beltman, The Airflow and Acoustic Performance of current 92mm system fans, Proceedings of Noise Con 2003.

Using Electrical Capacitance to Evaluate the Thermal Mechanical Stability of Thermal Interface Materials

Lauren Boston and Andrew Yu*, **Timothy Chainer and Edward Yarmchuk** (retired)+, **Michael Gaynes** (retired)*+

**Binghamton University*, 4400 Vestal Parkway East, Binghamton, NY 13902
+*BM T. J. Watson Research Center*, 1101 Kitchawan Road, Yorktown Heights, NY 10598
*+*Universal Instruments Corporation*, 33 Broome Corporate Parkway, Conklin, NY 13748

Lauren Boston | lboston1@binghamton.edu
Lauren Boston graduated from Binghamton University with a BS degree in mechanical engineering in May, 2017. Her senior project consisted of using mechanically representative hardware and electrical capacitance to evaluate the thermal mechanical stability of thermal interface materials. She is currently working for IBM Corporation, Poughkeepsie, NY.

Andrew Yu | ayu19@binghamton.edu
Andrew Yu graduated from Binghamton University with a BS degree in computer engineering in May, 2017 and an MS degree in electrical engineering in May, 2018. For his senior project, he coded and assembled the data acquisition system for the thermal mechanical monitoring of thermal interface materials using mechanically representative hardware and electrical capacitance.

Timothy Chainer | tchainer@us.ibm.com
Timothy Chainer is a Principal Research Staff Member at the IBM T.J. Watson Research Center and leads a team on Subsystem Cooling and Integration. As Principal Investigator of the IBM DARPA ICECool Fundamentals and Applications programs he led the development of Embedded Two-Phase Cooling for High Performance Computing. He was also Principal Investigator of the IBM DOE program on Economizer Based Data Center Liquid Cooling. He is a Senior Member of the IEEE and a member of the IBM Academy of Technology. He has over 200 Patents and has co-authored more than 40 technical papers. Dr. Chainer received his PhD in Low Temperature Experimental Physics from Rutgers University.

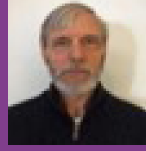

Edward Yarmchuk | edward.yarmchuk@gmail.com
Edward Yarmchuk retired from IBM T. J. Watson Research Center as a Research Staff Member in 2009, having worked at IBM for 28 years. He currently develops camera trap technology for Panthera, a wildlife conservation organization dedicated to preserving large cats in the wild. Dr. Yarmchuk received his PhD in Low Temperature Physics from Rutgers University.

Michael Gaynes | gaynesma@gmail.com
Michael Gaynes retired from IBM T. J. Watson Research Center as a Senior Technical Staff Member in 2016, having worked at IBM for 37 years. He held technical leadership positions that covered a wide spectrum of electronic packaging in manufacturing and development. He is currently working as a Process Research Engineer for the Advanced Process Lab at Universal Instruments, Inc. He is a coauthor on 50 technical publications and has over 150 US patents issued. He received a BS degree in Chemical Engineering from Brigham Young University.

INTRODUCTION

To improve cooling of electronic components, a heat spreader is typically attached to the component to spread the heat laterally and facilitate the heat removal by a heat sink. To ensure good thermal conduction between the heat spreader and heatsink, a thermal interface material is applied between the mating surfaces. During operation, changes in temperature of the electronic components, heat spreaders, heat sinks and circuit board result in thermal expansion which places stress on the thermal interfaces. Therefore, to ensure a reliable thermal solution, it is important to quantify the mechanical stability of the thermal interfaces. In many cases, the thermal interface material is non-conductive (electrically) with a dielectric constant which can be easily measured. This allows electrical capacitance to be used to monitor the thermal mechanical stability of thermal interface materials (TIMs) between a component heat spreader and heat sink. The component heat spreader and the heat sink provide parallel plates of a capacitor with the TIM in between as the dielectric. The measurement of capacitance is straightforward, fast and accurate (+/-0.08%) [1, 2].

CAPACITANCE AND THERMAL RESISTANCE CORRELATE

As shown in *Equations (1)* and *(2)*, thermal resistance (R) and the inverse of electrical capacitance (1/C) have the same geometric dependence on TIM bond line (BL) and area (A). In equation (1), the thermal resistance R (given by temperature gradient ΔT divided by the heat conduction rate Q) is equal to the TIM bond line (BL) divided by the thermal conductivity (k) and area (A). In equation (2), the inverse electrical capacitance (C) is equal to the TIM bond line (BL) divided by the permittivity of free space (ε_o), the relative dielectric constant (ε_r) and area (A). Therefore, the electrical capacitance between the component heat spreader and either the chip within the component or an external heat sink can provide a direct probe of the bond line thickness and material integrity of the dielectric TIM.

$$R = \frac{\Delta T}{Q} = \frac{BL}{kA} \quad (1)$$

$$\frac{1}{C} = \frac{BL}{\varepsilon_r \varepsilon_o A} \quad (2)$$

To demonstrate the correlation between capacitance and thermal resistance, samples were made of two 12.7 mm diameter aluminum rods of length 50 mm aligned end-to-end in a V- block with TIM in between. The bond line of the TIM was measured with a micrometer and the capacitance was also measured. Next, thermal resistance was measured in a thermal rod test apparatus previously described [3]. *Figure 1* shows the plot of unit area thermal resistance vs inverse capacitance with excellent correlation.

In commercial integrated circuit packages, the chip and heat spreader thermal conductivities are typically much higher than that of the TIM, but not infinite, so lateral gradients can be significant and the analogy to the electrical situation will be imperfect. Therefore, capacitance cannot be used as a substitute for detailed thermal modeling and measurement of packages. However, overall heat spreader to chip capacitance does reflect the average thermal conductance of the TIM and will track variations in thermal performance of parts. *Figure 2* illustrates this for a group of Flip Chip Plastic Ball Grid Array (FCPBGA) thermal test modules where capacitance and thermal resistance were measured. The capacitor plates in this measurement were the copper heat spreader and the silicon thermal test chip. The FCPBGA modules were solder attached to printed circuit cards. Probing the copper heat spreader was direct. The chip was accessed by probing the card connections to the chip heaters that were connected together. Included in the capacitance measurement are the series capacitance from the dielectric layer in the chip that separates the chip circuitry from the bulk silicon, and the parallel stray capacitance between the heat spreader and the substrate wiring. Both of these vary < 5% part to part and can be measured separately to be subtracted from the total capacitance measured, if desired. As *Figure 2* shows, there is good correlation between thermal resistance and inverse capacitance. Thus, capacitance provides a very simple means of tracking overall thermal performance among groups of parts.

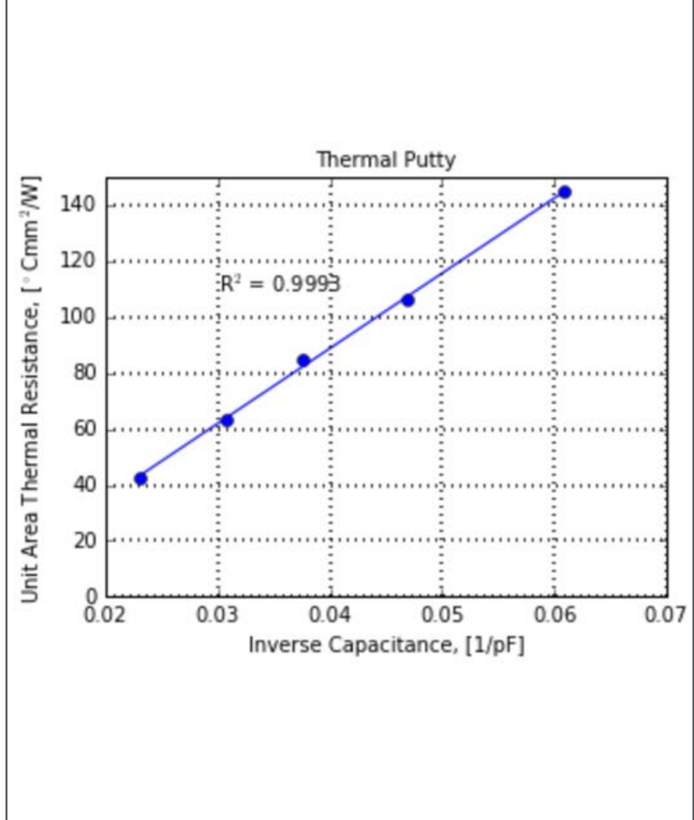

Figure 1: Plot of unit area thermal resistance vs inverse capacitance measured on aluminum rod samples.

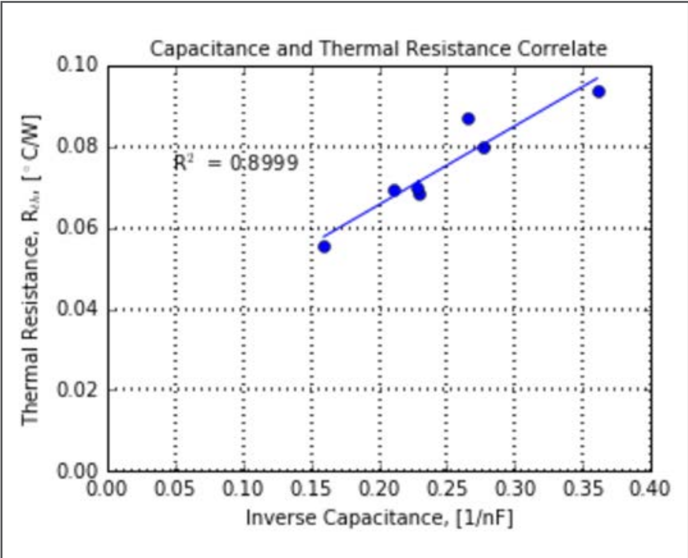

Figure 2: Plot of thermal resistance vs inverse capacitance measured on thermal test FCPBGA modules attached to cards.

When printed circuit board (PCB) assemblies with TIMs are subjected to environmental stress tests such as thermal cycling, damage can occur in the TIM. The damage can include pump-out, voiding, cracking, delamination and fracture which all result in a change of capacitance. In this damaged state, the TIM is not uniform in either thermal conductivity or dielectric constant. In the case where the damaged TIM has regions that are continuous from one interface to the other and is interspersed with missing material due to voids, cracks or pump out, the change in capacitance will be a good indicator for the change in thermal resistance as shown in *Figure 2.* The measured capacitance of the damaged TIM can be used with the dielectric constant to calculate a new capacitance bond line for comparison to the starting undamaged capacitance bond line. The percent increase in capacitance bond line is a good indicator for an expected increase in thermal resistance. It is important to emphasize that the bond line has not actually changed, rather the TIM within the bond line has changed due to the presence of air (missing TIM). The dielectric constant has changed to a composite of the TIM and air dielectric constants. Similarly, the thermal conductivity in the damaged TIM is a composite of the TIM and air thermal conductivities which is expected to result in similar fractional changes in both inverse capacitance and thermal resistance.

If the TIM were to delaminate from one interface or fracture, the thermal resistance change would be much higher than the capacitance change. In a split geometry with an air layer and a TIM layer, the effect of the air layer is much larger for thermal resistance than it is for capacitance because the TIM and air thermal conductivity ratio (~230) is much greater than the dielectric constant ratio (~10). Therefore, the capacitance bond line should not be used to quantify a percent increase in thermal resistance. An indication of delamination or fracture in the capacitance curve should appear as a sudden decrease, similar to the sudden drop in load for mechanical strength testing that is characteristic of fracture. Careful visual inspection of the TIM after separating the heat sink from the component at the end of testing should show predominantly planar fracture surfaces with little to no evidence of cracks or pump-out.

USING CAPACITANCE AS AN INDICATOR FOR THERMAL RESISTANCE ON MECHANICALLY REPRESENTATIVE HARDWARE

Many TIMs are low molecular weight organic polymers with no cross linking, such as thermal greases and phase change materials, or with light cross linking such as putties, gels and pads. The organic polymer is also highly filled with thermally conductive fillers. While compliance is a desired property in TIMs, if too high (as in a grease) results in material movement during thermal cycling. As filler content increases to achieve lower thermal resistance, compliance decreases. Too little compliance allows thermal mechanical stresses to build that can result in fatigue failure that includes fracture and delamination. Material responses such as long term adhesion and cyclical thermal mechanical loading require experimental study, especially if environmental aging and cyclic loading have cumulative damage effects. To understand material changes over a design lifetime and to enable effective virtual qualification, physical experiments are needed during the early design phase [4].

Previously, electrical capacitance was used to monitor the stability of TIMs using product development hardware that was designed, procured and assembled, taking several months [5]. A more recent study used a blank FR4 board, component heat spreaders and a large aluminum plate as a common heat sink. All parts were procured in less than two weeks [3]. Component heat spreaders were bonded on the FR4 board. Thermal interface materials of interest were dispensed on every component heat spreader and interfaced to the aluminum common heat sink. This mechanically representative design took only weeks to assemble compared to months to obtain early development hardware. Therefore, this new approach can provide an early evaluation of the thermal and mechanical design to either identify problems or confirm an acceptable design.

Figure 3 (a) shows an isometric view of the blank FR4 board, 440×590×6.4 mm, representative in size of many commercial applications. Depicted along the diagonals are the locations for the component heat spreaders, typically used on processor and ASIC modules. The heat spreaders were bonded with a room temperature curing structural adhesive to the FR4 board along the diagonals at distances from the center neutral point (DNP) of 50, 125, 200 and 275 mm. The aluminum common heat spreader, 440×590×6.4 mm, was thermally interfaced to the component heat spreaders and fastened to the FR4 board at locations depicted by the blue dots in *Figure 3 (b).* A spacer was located at every screw location and used to define a fixed bond line between the FR4 board and common aluminum heat sink that resulted in a design bond line of 0.5 mm. The resulting shear strains in the TIM at 100 °C, the peak temperature during thermal cycle testing, were 0.05, 0.13, 0.2 and 0.27.

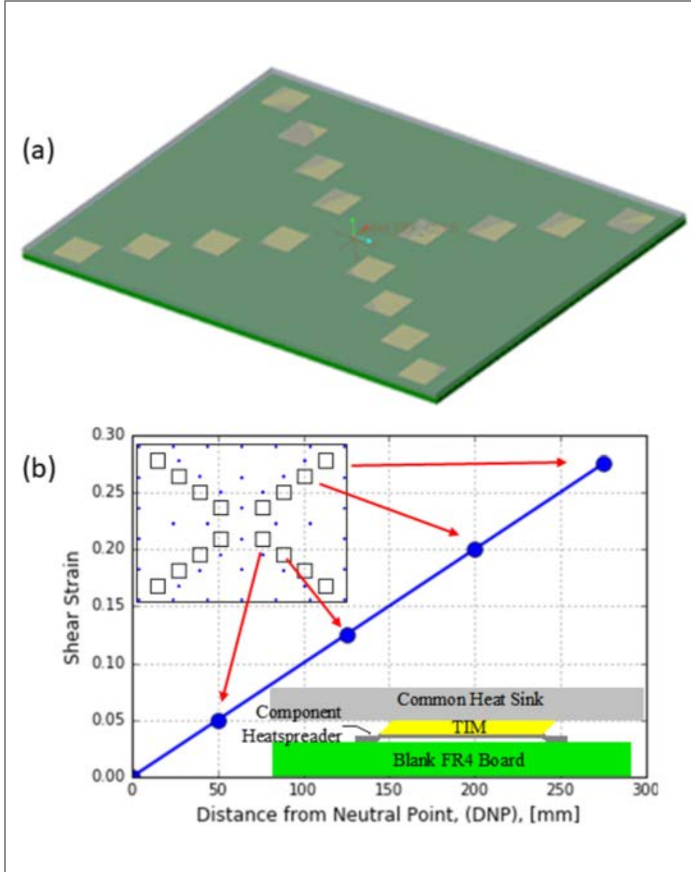

Figure 3. (a) Isometric view of the FR4 board and component heat spreader positions along the diagonals. (b) Plan view of FR4 board with heat spreader positions as open squares and screw locations as blue dots with plot of shear strain in the TIM vs. DNP on the FR4 board.

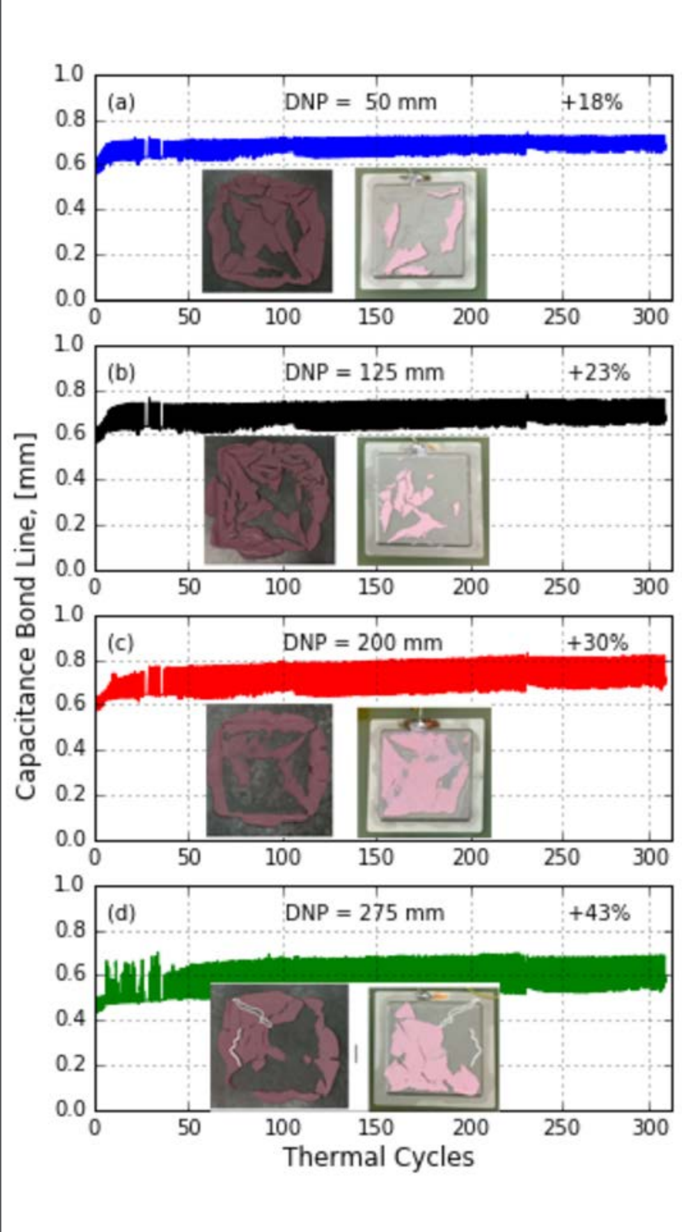

Figure 4. Thermal putty TIM A capacitance bond line plots and photos after separation. Left photo is the common aluminum heat sink and the right photo is the component heat spreader.

RESULTS AND DISCUSSION

During the thermal cycle between 0 and 100°C, the capacitance increased with temperature from 25°C to 100°C, indicating that the TIM was being compressed. The capacitance decreased during the cold portion of the thermal cycle at 0°C, indicating that the TIM was being pulled in tension [3].

The thermal cycle test results for a thermal putty, TIM A, appear in *Figure 4*, which includes a plot of the capacitance bond line vs. thermal cycles and photos of the TIM after the aluminum common heat sink was separated from the component heat spreaders. As discussed in Section 2, with damage to the TIM, the dielectric constant is a composite of the TIM and air dielectric constants. However, to quantify the impact of the change in capacitance, we use the TIM dielectric constant to calculate a new capacitance bond line that is different from the initial bond line, understanding that the physical bond line has not actually changed. The photos in *Figure 4* clearly show damage in the TIM in the form of voids and cracks caused by TIM movement during the test. The plots in Figure 4 also show the capacitance baseline bond line increasing with cycles with greater peak to valley changes as the DNP increases.

The initial capacitance bond line for *Figure 4 (a)* was 0.61 mm and the reduction in capacitance during the first 25 thermal cycles is equivalent to a bond line that increased to 0.67 mm (10%), indicating that structural change had occurred in the TIM. Between cycles 25 and 300, the continued decrease in capacitance is equivalent to a further increase in bond line from 0.67 mm to 0.72 mm for a total increase of 18%. The heat spreaders at the higher DNPs experienced higher increases in the capacitance bond lines of 23%, 30% and 43%, respectively in *Figure 4 (b), (c)* and *(d)*, consistent with the expectation that increasing strain will accumulate more damage in the TIM.

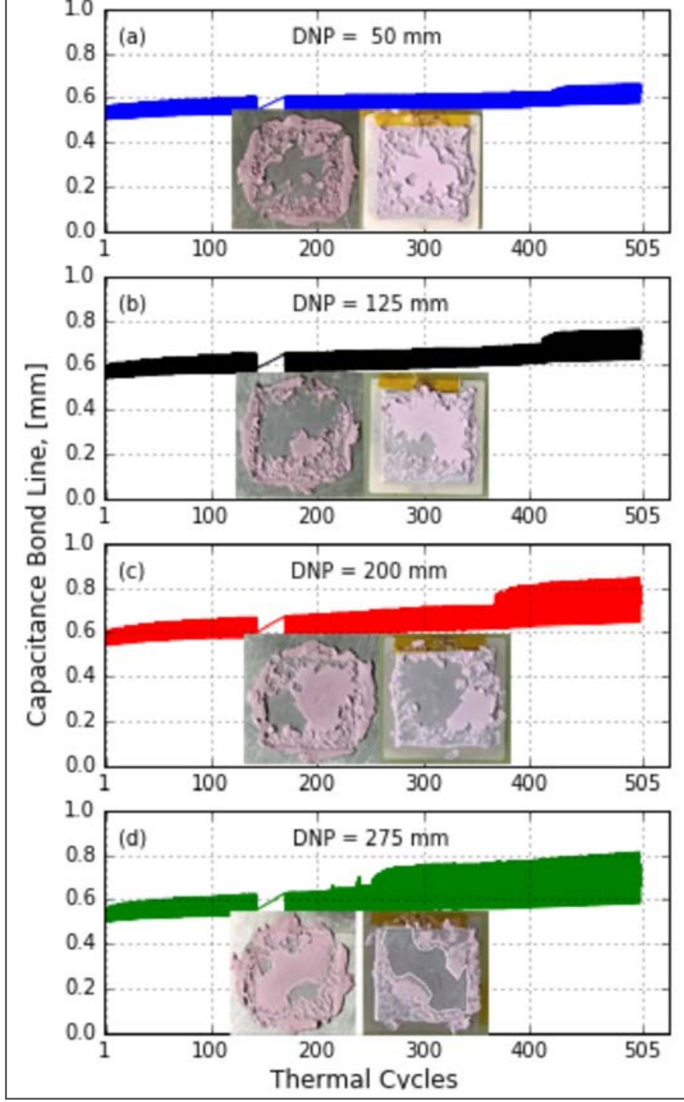

Figure 5. Thermal putty TIM B capacitance bond line plots and photos after separation. Left photo is the common aluminum heat sink and the right photo is the component heat spreader.

The photos in the plots show the separated TIM surfaces presented in an opened book manner. In *Figure 4 (d)*, white tracing is used to highlight where TIM is missing on both the heat sink and the heat spreader surfaces. Careful study of the photos reveals that similar cracks in the TIM exist at all heat spreader locations on the FR4. The presence of cracks and voids results in the thermal conductivity being a composite of the TIM and air thermal conductivities, lowering the average thermal conductivity in the bond line and indicating an accompanying increase in the bond line thermal resistance.

The thermal cycle test results for a second thermal putty, TIM B, appear in *Figure 5*. Evident in all four plots is a sudden increase in the capacitance bond line (sudden decrease in capacitance) that appears at ~250 thermal cycles at the highest DNP and progressively later to ~425 cycles at the lowest DNP. Inspection of the TIM surfaces after disassembly shows large areas as indicated by the white tracing in *Figure 5 (d)* that appear to be delamination of the TIM near the interface of either the aluminum or component heat spreader. This observation is consistent with the sudden increase in capacitance bond line as delamination results in a sudden drop in capacitance. As previously described in Section 2, when delamination of the TIM occurs the capacitance bond line should not be used to quantify a percent increase in TIM thermal resistance since the thermal resistance change would be much higher than the capacitance bond line change. More importantly, the results demonstrate that TIM B is very susceptible to thermal mechanical break down and should not be used in applications exposed to thermal cycling shear strains that exceed 0.05.

CONCLUSIONS

Electrical capacitance is an effective indicator for thermal resistance characterization. Mechanically representative hardware is simple, fast and inexpensive to procure, very early in a development program compared to the long lead time and expense to design, procure and assemble early production, thermally testable hardware. TIM candidates can be ranked and the effectiveness of a thermal solution can be assessed. Early discovery of deficiencies allows time for material, design and process changes.

ACKNOWLEDGMENTS

Dr. James Wilcox, Area Array Consortium, Universal Instruments Corporation and Prof. David Klotzkin, Binghamton University, for their guidance and support of this Senior Engineering Project at Binghamton University.

REFERENCES

[1] Gaynes, M. A. and Yarmchuk, E. J., “Process for Measuring Bond Line Thickness,” US Patent 776409B2, Jul. 27, 2010.

[2] Chainer, T. C., Gaynes, M. A. and Yarmchuk, E. J., “Using In situ Capacitance Measurements to Monitor the Stability of Interface Materials in Complex PCB Assemblies and Other Structures,” US Patent 8589102B2, Nov. 19, 2013.

[3] Boston, L., Yu, A., and Gaynes, M., “Using Electrical Capacitance and Mechanically Representative Hardware to Monitor the Thermal Mechanical Stability of Thermal Interface Materials”, SemiTherm 34, San Jose, CA, March 2018.

[4] Doman, J., Kobeda, E., Bielick, J., Kuczynski, J., Tofli, T. and Vaughn, M., “Evaluation of Thermal Interface Material Performance in a Cyclic Strain Environment”, Proceedings of the Surface Mount Technology Association, International (SMTAi) Conference, Florida, October 24-28, 2010.

[5] Gaynes, M., Chainer, T., Yarmchuk, E., Torok, J., Edwards, D., Olson, D. and Pizzolato, K., “Using In situ Capacitance Measurements to Monitor the Stability of Thermal Interface Materials in Complex PCB Assemblies”, IMAPS Conference, Raleigh, NC, 43rd International Symposium on Microelectronics, pp. 450-457, November, 2010.

THERMAL MEASUREMENT, MODELING AND MANAGMENT

SYMPOSIUM AND EXHIBITION

MARCH 18TH - 22ND 2019

SAN JOSE, CALIFORNIA AT THE DOUBLETREE BY HILTON

REGISTER NOW!
WWW.SEMI-THERM.ORG

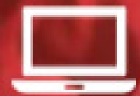

SEMI-THERM 35

EXHIBITION WITH OVER 40 VENDORS AND VENDOR WORKSHOPS

EXPERT-REVIEWED PAPERS PRESENTED BY THE BRIGHTEST THERMAL PROFESSIONALS AND EDUCATORS

TECHNICAL SESSIONS

LED
Two-Phase Cooling
Thermal Interface Materials
Automotive / Aerospace /Outdoor

Measurement Techniques
CFD / Numerical Modeling
Consumer Electronics
Data Center Cooling

NETWORKING OPPORTUNITIES

PRE-CONFERENCE SHORT COURSES

CAN'T ATTEND SEMI-THERM 35?

SAVE THE DATE

SEMI-THERM 36

MARCH 16TH - 20TH 2020

WWW.SEMI-THERM.ORG

Special Challenges In 3D Simulations of Graphite Heat Spreaders

Rick Beyerle
NeoGraf Solutions, LLC

INTRODUCTION

Graphite is a naturally occurring form of pure carbon in which the atomic bonds interlock in the layers of a two-dimensional molecular sheet. In nature, dense, rigid graphite ore is mined, purified, and processed into numerous applications, including the inexpensive flexible natural graphite sheets used in electronics. The ore is mechanically reduced and then reconstructed into flexible sheets that typically range from 40μm to several millimeters in thickness. Because of this alignment process, the ability to conduct heat both in-plane and thru-plane can be engineered to the final application, such as heat spreader, heat shield, or thermal interface material (TIM). Chemical vapor deposition is a precise, but relatively expensive, means of assembling carbon atoms into highly oriented pyrolytic graphite (HOPG) in a controlled atmosphere. HOPG tends to be rigid and many millimeters in thickness. For the high volume manufacturing used in electronics, methods have been developed to synthesize thin flexible graphite heat spreaders from polymers. These techniques produce sheets on the order of 10 to 50μm, fully compressed, although less dense versions used as thermal interface materials are available. The thinnest form of graphite, graphene, is a planar carbon molecule one or two atoms thick. Because all flexible graphite is pure carbon, it remains flexible hundreds of degrees above and below ambient, so its practical application in electronics is limited only by the adjacent materials such as adhesives and dielectrics.

SIMPLE ORTHOTROPIC CALCULATIONS

The Scale of Graphite Thermal Orthotropy

For most electronics-scale applications, both natural and synthetic graphite foils present as homogeneous, orthotropic solids. Synthetic graphite sheets, in particular, remain homogeneous down to the molecular level, to the point that they are used as monochrometers in X-ray diffraction studies. In contrast, natural graphite foils are compressed from graphite flakes [1] and contain varying degrees of anisotropy below one-quarter millimeter length scales. The thermal properties needed for steady state calculations (thermal conductivity) and for transient calculations (heat capacity and density) vary measurably with grade, thickness, and operating temperature. Because the thermal conductivity is measured at room temperature, a correction may be applied for electronics-operating temperatures. In particular, some graphite vendors rate their products based on room temperature measurements, while others rate them based on operating temperature calculations [2].

An important scale for modeling graphite is the ratio of thermal conductivity in-plane to thru-plane. Grades are manufactured according to their intended use, but most grades have more than 100 times the thermal conductivity in-plane to thru-plane. *Table 1* shows some representative values.

Table 1
Typical natural and synthetic graphite properties by application

Application	Thickness	K_{xy}	K_z	R_z	K_{xy}/K_z
	μm	W/m·K	W/m·K	°C/cm²·W	n/a
Spreaders					
NG	40-940	400	3.7	n/a	108
SG	40	1350	3.4	n/a	397
SG	17	1500	3.4	n/a	441
TIMs					
110 kPa NG	51-127	240	6	0.5	40
200 kPa SG	200	800	7	0.5	114
700 kPa SG	50	800	7	0.2	114

NG=Natural, SG=Synthetic Graphite
C_p=71 kJ/kg·K at room temperature
ρmax = 2.26 g/cm3 , grades vary

Rick Beyerle | rbeyerle@neograf.com
Rick Beyerle is a senior development engineer and heat transfer specialist at NeoGraf Solutions, LLC, which was formerly the advanced electronics materials division of GrafTech International. Rick is responsible for developing measurement and modeling techniques for graphite heat spreaders, TIMs, and gap pads, as well as non-electronics applications of graphite. His work on SpreaderCalc, a web-based app for simulating heat flow in highly anisotropic graphite foils, was featured in IEEE Spectrum and NASA Tech Briefs. *This article was excerpted from "Development of Heat Transfer Tools for Sizing Flexible Graphite Spreaders in Mobile Applications" delivered at the ASME InterPACK 2015.*

Table 2							
Relative aspect ratios and calculated device temperature (Tj) for typical 0.250mm NG and Al heat spreader example.							
Number of Grid Layers	Length per cell (mm)	Height per cell (mm)	Length/ height ratio (X/Z)	Kxy/Kz mat'l ratio	K/ aspect ratio	Tj (˚C)	$\frac{Tj - Tj_{Grid\ Max}}{Tj_{Grid\ Max} - T_{Air}}$ (%)
NG SS400-250 (Kxyz = {400, 400, 3.7}; ε=0.96)							
1	0.43	0.25	1.7	108	62.7	75.5	11.3%
2	0.43	0.125	3.5	108	31.3	71.9	4.2%
4	0.43	0.063	6.9	108	15.7	70.4	1.0%
8	0.43	0.032	14	108	7.8	68.3	-3.2%
16	0.43	0.016	28	108	3.9	69.9	0.2%
32	0.43	0.008	55	108	2	69.9	0.0%
AL3003 (Kxyz = {159, 159, 159}; ε=0.25)							
1	0.43	0.25	1.7	1	62.7	89.2	1.45%
2	0.43	0.125	3.5	1	31.3	88.2	-0.01%
4	0.43	0.063	6.9	1	15.7	88.2	0.00%
Device Power = 3.4 W; Air temperature = 20˚C; Natural Convection Cooling; Vertical Orientation of Spreader							

Two challenges arise from these extreme ratios; both the accuracy of the answer and the reliability of convergence will be challenged. *Table 2* shows the length-to-height ratios of the hexahedral grid elements taken from a model and the relative size compared with the thermal orthotropy of the graphite.

The takeaway is that a model meshed for graphite may not converge if used for metals, and vice versa, due to the distortion that results from the orthotropic thermal conductivity ratios. Moreover, a "smaller" or finer grid will not improve the accuracy; it is the aspect ratio of the elements near the source that drives the solution.

Grid Dependency in a CFD Model

Low aspect ratio discretization is not a pure function of geometry as it is in isotropic materials, and a mesh suited for aluminum may not be optimized for graphite. In isotropic solids, a unit aspect ratio mesh is less likely to distort a calculation, and many automatic meshing algorithms do a fine job with isotropic materials. It is up to the modeler to determine whether the tool includes algorithms to automatically increase the mesh density in regions of high gradients, which may be coded differently for solid and fluid volumes. Due to the thin nature of graphite heat spreaders, substantial Z-axis magnification may be useful in viewing the model near the heat source for the modeler to observe the effect of discretization near the (expected) gradients. Magnifying only the through-thickness geometry, rather than zooming in, helps to retain perspective in these very thin layers. If the modeler exchanges an isotropic material property for a graphite material property, or vice versa, without re-gridding, the model may fail to converge. A provision for plate elements, which are included in some FEA software, may simplify this step in planar models.

To quantify the effect of the grid aspect ratios, a simple model was constructed and meshed identically for 250μm sheets of two heat spreading materials. Standard grades of graphite (SS400-250 [3]) and aluminum (3003-H14) were used to spread the heat generated by a surface-mounted electronic device.

Thermal Model

The thermal model was constructed, using commercial finite-volume CFD software.[4] Its details replicated the mounting of a single LED mounted atop a 50mm x 50mm x 250μm thick heat spreader. The 3.5mm heat source is bonded to the center of the graphite plate atop a dielectric material except for the thermal via. A polymer dome and quartz diffuser make up the top of the LED, and the base consists of GaN with material properties published by the manufacturer. [5,6] The test setup was described and was used for model validation in a separate publication.[7]

Figure 3 depicts the component geometry in cross-section with the calculated heat flux superimposed on it. The model was used to calculate component temperatures for a graphite material with an in-plane thermal conductivity 108 times that of the thru-plane value (Kxy/Kz = 108). Solutions were performed using grid cell sizes of varying aspect ratio.

Thermal Model Results and Discussion

Table 2 indicates the details of 6 iterations of the solution, which differed according to the number of grid layers in the graphite material and, consequently, the cell height. It also provides the calculated value of Tj (maximum heater temperature) and the % difference in Tj for each iteration, compared with the 32-layer solution, assumed to be the most accurate iteration. It also shows 3 iterations for an identical model, with the exception that the graphite is replaced by aluminum.

The highest temperature in the model, which fell within the square footprint of the heat load, was chosen as the junction temperature, and a point opposite it on the back side of the spreader was used as a touch temperature. The vertical plate was modeled in a laminar natural convection environment. Surface temperatures were sampled along the horizontal rather than vertical axis to reduce the influence of convection.

The grid layers in the space between the top and bottom planes of the heat spreader were manually specified, as were the planes normal to them bounding the footprint of the device. The mesher automatically added cells adjacent to the heat source, presumably due to the proximity of non-aligned edges in the under-meshed models, and round-off errors. A typical temperature error, shown as a percent difference from the most refined mesh, was calculated for *Table 2*. The results revealed insensitivity to grid layers in the aluminum control model, but decreasing temperature (spreading resistance) as the number of layers was increased in the graphite. For the junction temperature (Tj), the biggest return on computing memory to solution accuracy occurred when increasing from one to three layers, but a 2.3% error was still apparent in the case temperature with a four-layer mesh. This mesh induced error continued in the solder-point temperature atop the dielectric (Tsp), as well as in a touch temperature on the opposite side of the spreader (Ttouch). However, grid dependency did not appear on the surface 25mm away from the source.

Figure 1 depicts temperature contours of the full model in a perspective view. The CFD capability of the software is used to calculate the cooling effect of buoyancy-driven natural convection air currents and the resultant temperatures on the components.. It also shows the overall geometry of the LED device in contact with the two electrical pads on the substrate.

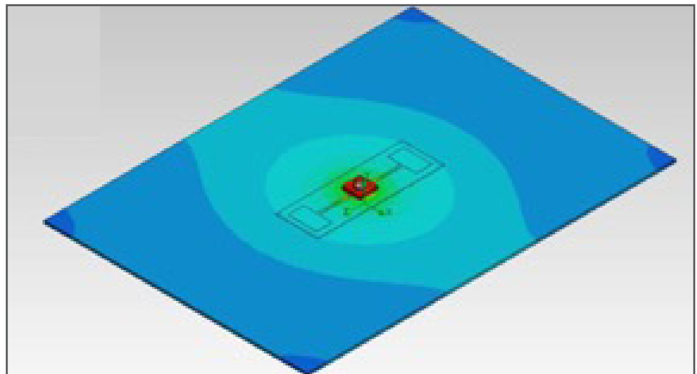

Figure 1. Physical configuration of model with LED atop electrical leads and dielectric layer on a large graphite spreader plate. Temperature contours are shown for a vertical plate orientation. Temperatures: Peak (Red) = 77.5 ˚ C; Minimum (dark blue) = 56.9 ˚ C; Air = 20 ˚ C.

Figure 2 shows temperature contours mapped onto the device and spreader vertical cross-section. The graphite is meshed with 2 grid layers. As *Table 2* indicates, the calculated value of Tj differs from the most refined model having 32 grid layers by 4.2% of the Tj temperature rise above the ambient air temperature.

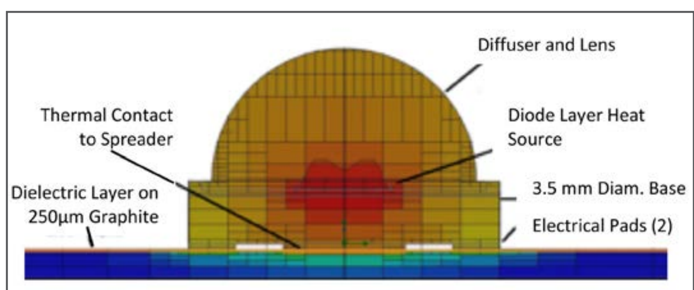

Figure 2. Vertical slice through the thermal model with LED atop electrical leads and dielectric layer on a large spreader plate. Graphite meshed with 2 grid layers. Temperature contours are shown for a vertical plate orientation. Temperatures: Peak (Red) = 68 ˚ C; Minimum (dark blue) = 48 ˚ C; Air = 20 ˚ C.

Figure 3 displays heat flux contours on the vertical cross-section of the component geometry. Here, the graphite has the maximum number of grid layers, equal to 32. The heat flux profiles in *Figure 3* reveal that the spreading in the graphite extended to many times the thickness of the spreader and well beyond the heat source footprint. In this example, a single layer mesh will capture most of the spreading in the isotropic material.

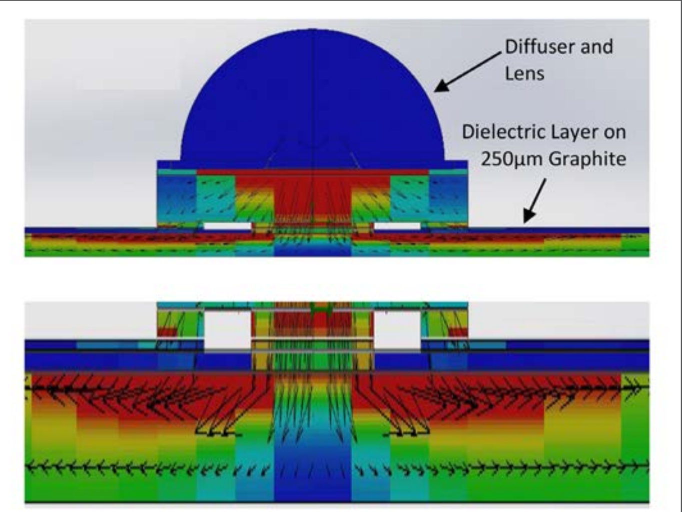

Figure 3. Top: Vertical slice through the thermal model of an LED mounted on graphite spreader. Heat flux contours are shown. Graphite meshed with 32 grid layers. Bottom: Magnification (@ 5.3x) of the spreader in the z-direction reveals flux gradients within the graphite layer, that may aid in selecting an optimum grid layer thickness.

In order to capture the heat flux profile adjacent to the surface heat source, the analyst must balance the need for a high orthotropic ratio grid with a narrow grid that also captures the edges of the source. This two-dimensional drive for granularity may result in some very tiny, high aspect ratio cells directly adjacent to the source. Depending on the meshing or gridding technique, it may be useful to create an inset part in the spreader and impose a fine mesh on it locally.

CONCLUSIONS

Modeling graphite heat spreaders is within the capability of commercial software packages but the user needs to be aware of the unique capabilities and limitations of the numerical methods. High orthotropic-ratio flexible graphite heat spreaders and TIMs impart a more disproportionate thermal influence than their thin geometry would suggest. The validation of a thermal simulation should be accurate enough to distinguish differences in thickness and materials, and may require scrutiny of the energy balance within very fine structures that might otherwise be neglected. These high orthotropic ratios account for the occasional failure of models discretized for graphite to fail when converted to an isotropic material, and vice versa.

REFERENCES

1. Shane, James H., Robert J. Russell, and Raymond A. Bochman. "Flexible graphite material of expanded particles compressed together." U.S. Patent 3,404,061, issued October 1, 1968.
2. Beyerle, R., Smalc, M., Wayne, R., & Reynolds III, R. A. (2013, July). "A Comparison of Methods to Measure the Thermal Diffusivity of Anisotropic Graphite Heat Spreaders." In *ASME 2013 International Technical Conference and Exhibition on Packaging and Integration of Electronic and Photonic Microsystems* (InterPACK2013-73093). American Society of Mechanical Engineers.
3. eGRAF®, SPREADERSHIELD™, and HiTHERM™, are trademarks of NeoGraf Solutions, LLC.
4. FloEFD®, trademark of Mentor (Version = that current in December, 2014).
5. Tseng, J.W., Getz, G., Fedor, B.S., Krassowski, D.W., 2000, "Anisotropic Graphite Heat Spreader for Electronics Thermal Management," *Proceedings, International PCIM/Power Quality Conference*, Nuremberg, Germany, June 6, 2000.
6. Norley, Julian. "The role of natural graphite in electronics cooling." Technical Brief, *ElectronicsCooling*, Vol. 7, No. 3, August, 2001).
7. Yin Xiong *et al.*, "Thermal tests and analysis of thin graphite heat spreader for hot spot reduction in handheld devices," *2008 11th Intersociety Conference on Thermal and Thermomechanical Phenomena in Electronic Systems*, Orlando, FL, 2008, pp. 583-590.

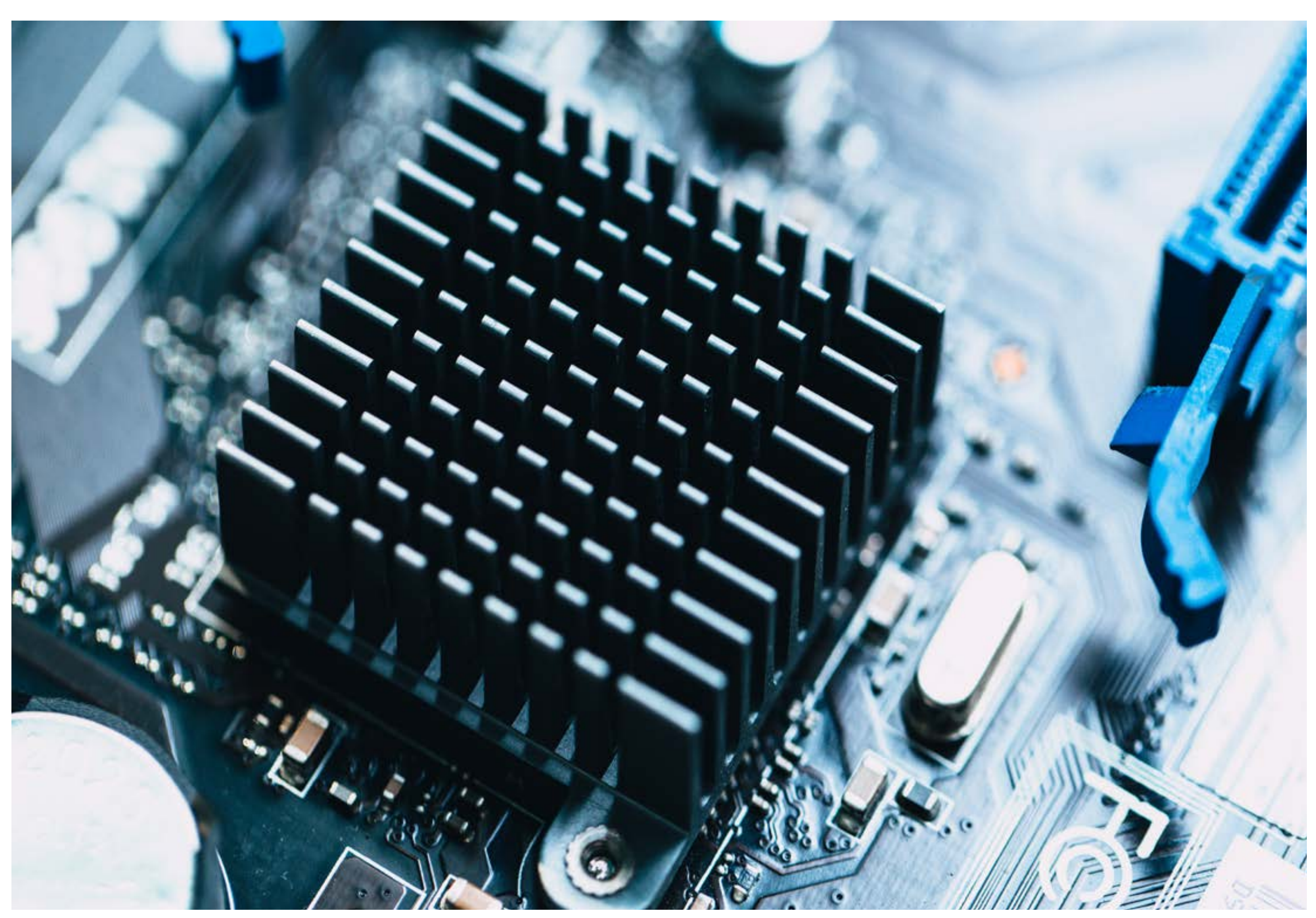

Index of ADVERTISERS

Alpha Novatech, Inc.
473 Sapena Ct. #12,
Santa Clara, CA 95054

t: +1 (408) 567-8082
e: sales@alphanovatech.com
w: www.alphanovatech.com
page: Inside Front Cover

CPC Worldwide
1001 Westgate Drive
St. Paul, MN 55114

t: (651) 645-0091
w: www.cpcworldwide.com
page: 5

ITEM Media
1000 Germantown Pike
Plymouth Meeting, PA 19462

t: (484) 688-0300
e: info@item.media
w: www.item.media
page: 13

Master Bond, Inc
154 Hobart Street
Hackensack, NJ 07601

t: +1 (201) 343-8983
e: main@masterbond.com
w: www.masterbond.com
page: 17

Mentor Graphics
8005 SW Boeckman Road
Wilsonville, OR 97070

t: (800) 592-2210
e: sales_info@mentor.com
w: www.mentor.com
page: 3

Polyonics, Inc.
28 Industrial Park Drive
Westmoreland, NH 03467

t: +1 (603)-352-1415
e: info@polyonics.com
w: polyonics.com/VeryCool
page: 9

SEMI-THERM 35
San Jose, California
March 18th – 22nd, 2019

t: +1 (408) 840-2354
e: drael@semi-therm.org
w: www.semi-therm.org
page: 23

Thermal Live™ 2019
Online Event
October 22nd – 23rd, 2019

t: (484) 688-0300
e: info@electronics-cooling.com
w: www.thermal.live
page: Back Cover

Call for Authors and Contributors!

Want to be a part of the next issue of Electronics Cooling? Have an article or blog post you'd like to write for Electronics-Cooling.com?

Let us know at
editor@electronics-cooling.com

electronics COOLING
www.Electronics-Cooling.com

October 22 – 23 2019

thermal LIVE 2019

ONLINE EVENT

The Largest Single Thermal Management Event of The Year - Anywhere.

Thermal Live™ is a new concept in education and networking in thermal management - a FREE 2-day online event for electronics and mechanical engineers to learn the latest in thermal management techniques and topics. Produced by *Electronics Cooling®* magazine, and launched in October 2015 for the first time, Thermal Live™ features webinars, roundtables, whitepapers, and videos... and there is no cost to attend.

For more information about Technical Programs,
Thermal Management Resources, Sponsors & Presenters

please visit:

thermal.live